NTIA Report 19-540

Interference Protection Criteria Simulation

Robert J. Achatz
Brent Bedford

report series

U.S. DEPARTMENT OF COMMERCE • National Telecommunications and Information Administration

NTIA Report 19-540

Interference Protection Criteria Simulation

Robert J. Achatz
Brent Bedford

U.S. DEPARTMENT OF COMMERCE

August 2019

DISCLAIMER

Certain commercial equipment and materials are identified in this report to specify adequately the technical aspects of the reported results. In no case does such identification imply recommendation or endorsement by the National Telecommunications and Information Administration, nor does it imply that the material or equipment identified is the best available for this purpose.

CONTENTS

FIGURES

TABLES

ABBREVIATIONS/ACRONYMS

AGC	Automatic gain control
AMC	Adaptive modulation and coding
AWGN	Additive white Gaussian noise
BLER	Block error rate
CBRS	Citizens Broadband Radio Service
CFAR	Constant false alarm rate
CQI	Channel quality indicator
CP	Cyclic prefix
CRC	Cyclic redundancy check
CW	Codeword
dB	Decibel
dBm	Milliwatt decibels
eNB	Evolved Node B
FDD	Frequency division duplex
FDR	Frequency dependent rejection
FEC	Forward error correction
FTC	Fast time constant
GN	Gaussian noise
HARQ	Hybrid automatic repeat request
INR	Interfering signal power to noise power ratio
IPC	Interference protection criteria
LTE	Long Term Evolution
MAC	Medium access control
Mbps	Megabits per second
MCS	Modulation coding scheme
ms	Millisecond
MTI	Moving target indicator
NA	Not available
OFDM	Orthogonal frequency division multiplexing
OFDMA	Orthogonal frequency division multiple access
PMI	Precoding matrix indicator
PRI	Pulse repetition interval
PRF	Pulse repetition frequency
PSD	Power spectral density
RB	Resource block
RCS	Radar cross section
RE	Resource element

RF	Radio frequency
RI	Rank indicator
RSSI	Received signal strength indicator
SINR	Signal power to interfering signal power plus noise power ratio
SNR	Signal power to noise power ratio
STC	Sensitivity time constant
TB	Transport block
TDD	Time division duplex
TM	Transmission mode
TTI	Transmit time interval
UE	User equipment
VSG	Vector signal generator

DEFINITIONS

Gaussian noise interfering signal: Interfering signal with Gaussian noise characteristics

Interference: Deleterious effect of interfering signal on system, e.g. speckles on television display.

Interfering signal: Undesired signal received by system.

Interference protection criteria (IPC): Maximum interfering signal power a system can tolerate without interference.

IPC measurement: Hardware implementation of IPC test using test fixture.

IPC simulation: Software implementation of IPC test using simulation models.

IPC test: Interference test from which IPC is derived.

EXECUTIVE SUMMARY

In today's spectrum sharing scenarios, interference is often allowed as long as the performance of the system experiencing the interference is not significantly degraded. Spectrum planners use distance and frequency separations between systems to minimize the probability of interference. The amount of separation is determined by the allowed performance degradation and corresponding interfering signal power, referred to as the interference protection criteria (IPC).

Because of the complicated interaction of interfering signal characteristics with receiver signal processing functions, IPC in general cannot be determined from frequency dependent rejection (FDR) formulas. Consequently, engineers at the National Telecommunications and Information Administration (NTIA) Institute for Telecommunication Sciences (ITS) often estimate IPC with measurements of operational equipment in the laboratory or field.

These measurements are often hindered by equipment unavailability and inaccessible intermediate signals, performance metrics, and operational parameters. These hindrances can make accurate and repeatable measurements difficult to obtain by ITS and other interested parties. The purpose of this research is to determine if radio system software simulation can accurately emulate these measurements and alleviate their hindrances.

Our approach is to use the commercial off-the-shelf (COTS) radio system simulator software to model previous IPC measurement test fixtures and compare simulated to measured results. Currently, there is considerable interest in Long Term Evolution (LTE) cellular radio systems sharing spectrum with Federal radars in the 3.5 GHz Citizen Broadband Radio System (CBRS) band. Consequently we have chosen to emulate IPC measurements for SPN-43C radar interference in LTE user equipment (UE) receiver and LTE evolved node B (eNB) interference in a SPN-43C radar receiver.

The LTE equipment measured used adaptive modulation and coding (AMC), hybrid automatic repeat request (HARQ) retransmission, and multi-antenna adaptation to mitigate attenuation, shadow fading, and multipath radio channel propagation effects. Conceivably, these mechanisms could also mitigate interference. The SPN-43C radar had a manually set fixed threshold. While the radar had some clutter rejection functions that could also potentially mitigate interference, they were disabled during measurements.

The LTE signal is organized into frames, subframes, and orthogonal frequency-division multiplexing (OFDM) words. The OFDM words contain channels and signals that periodically repeat every subframe or frame. Because the SPN-43C pulse repetition interval (PRI) was the same as the LTE subframe period, the SPN-43C radar interference in LTE UE test repeatedly interfered with the same channels or signals. Simulated SPN-43C interference in LTE UE results fell into two categories depending on which channels or signals were interfered with.

In the first category, where the pulse was repeatedly placed on the primary synchronization signal (PSS), the physical downlink shared channel (PDSCH) throughput decreased gradually with increasing interfering signal power. In the second category, where the pulse was repeatedly placed on the physical downlink control channel (PDCCH), physical downlink broadcast channel (PPCH), and secondary synchronization signal (SSS), PDSCH throughput decreased quickly, remained somewhat constant, then completely stopped with increasing interfering signal power.

The difference between the simulated results can be attributed to the AMC algorithm. The simulated AMC assessed channel quality by measuring PSS signal to noise ratio (SNR). In the first category, where the pulse was placed on the PSS, the AMC was able to match the modulation and coding scheme (MCS) to the interference conditions. Reduced throughput was due to changes in the MCS. In the second category, where the pulse was placed on the other channels and signals, the AMC was unable to match the MCS to the interference conditions and the interference could only be mitigated by HARQ retransmissions.

Measured results showed throughput quickly degrading to approximately half its maximum then gradually degrading to one-third its maximum with increasing interfering signal power. Measurements were performed without knowing which channel or signal the pulse was repeatedly placed on. While the measurement agrees most with simulations in the second category, it appears as though differences between AMC functions allowed the measured equipment to assign a more relevant MCS and continue operation at higher interfering signal powers.

It is interesting to note that other simulation and measurement results with Gaussian noise interference were similar. Consequently, it is conceivable that better measured SPN-43 interference throughput might have been made possible by a proprietary pulsed interference rejection (IR) algorithm whose performance improved with increased interfering signal power.

The LTE eNB signal was emulated with Gaussian noise in the LTE eNB interference in SPN-43C IPC test. The simulation results showed probability of false alarm (P_{fa}) and probability of detection (P_d) increasing with interfering signal power. These results are consistent with those of fixed threshold radars where interference manifests itself primarily as false alarms.

Due to problems accessing the radar's built in test function, the IPC measurement was conducted by the injection of test targets and visually counting the number discerned on the radar display. P_{fa} is too difficult to quantify visually so only P_d was measured. In stark contrast to the simulation results, the measurement result showed P_d decreasing with interfering signal power. This contradictory measurement result is most likely caused by targets being counted as missing when only obscured by false alarms.

The radio system software simulator provided most but not all functions needed to accurately emulate the equipment and IPC measurement method. Notable deficiencies include a lack of a LTE multi-antenna adaptation algorithm and AMC function options. Multi-antenna adaptation will become more important if regulators choose to estimate IPC in time-varying multipath. The AMC function should have the option to estimate SNR from the common reference signal (CRS) and take first transmission block error rate (BLER) into account when assigning the channel quality indicator (CQI).

IPC measurements are often conducted as if the measured equipment is a "black box" operating under "nominal conditions." However, with software simulation, the scope of the IPC test must be enlarged by the necessary selection of receiver models and their associated signal processing algorithms and parameter settings. Ultimately, integration of software simulation into the spectrum engineering process and acceptance by the spectrum engineering community will

depend on whether stakeholders find mutually-agreeable receiver models that can be feasibly implemented in today's COTS radio system simulator software.

In conclusion, rather than duplicate measurement results, the simulation results pointed out weaknesses in the measurement method. For SPN-43C interference in LTE UEs the simulation pointed out the importance of pulse placement within the LTE subframe. Clearly more measurements are needed with different pulse placements. For LTE eNB interference in the SPN-43C radar the simulation showed that IPC should be estimated from the P_{fa} rather than the P_d.

We found software simulation removed most measurement hindrances. Besides being readily available, the radio system software simulator provided almost unlimited access to the intermediate signals and performance metrics needed for IPC tests. These advantages can potentially enable engineers to identify vulnerable subsystems and recommend ways to make their operation more robust in the presence of the interfering signals.

With these considerations, we recommend more resources be devoted to the development of receiver models mutually agreeable to all spectrum-sharing stakeholders, so that IPC simulations can immediately supplement and someday replace IPC measurements.

INTERFERENCE PROTECTION CRITERIA SIMULATION

Robert J. Achatz[1] and Brent Bedford[2]

Interference protection criteria (IPC) determine the interfering signal power a system can tolerate when sharing spectrum with other services. IPC are typically determined by measurements, but good measurements are often hindered by restrictions on equipment availability and inaccessible intermediate signals, performance metrics, and operational parameters. The purpose of this research is to determine if radio system software simulation can accurately emulate these measurements and alleviate their hindrances. Our approach is to use commercial off-the-shelf (COTS) radio system simulator software to model previous IPC measurement test fixtures and compare simulated to measured results. Measurements of mutual interference between SPN-43C radar and LTE systems are compared. The comparison revealed that 1) when the SPN-43C pulse repetition interval was the same as the LTE subframe period SPN-43C interference in the LTE UE was highly dependent on which OFDM word within the LTE subframe the SPN-43C pulse was repeatedly placed on and 2) simulation is more accurate than measurement for IPC tests with fixed threshold radars such as SPN-43C. These revelations show that simulation is a useful addition and potentially viable alternative to IPC measurement.

Keywords: Citizens Broadband Radio Service, electromagnetic compatibility analysis, interference protection criteria, LTE, radio system software simulation, spectrum engineering, spectrum sharing, surveillance radar

1. INTRODUCTION

In today's spectrum sharing scenarios, interference is often allowed as long as the performance of the system experiencing the interference is not significantly degraded. Spectrum planners use distance and frequency separations between systems to minimize the probability of interference. The amount of separation is determined by the allowed performance degradation and corresponding interfering signal power, referred to as the interference protection criteria (IPC) [1].

Because of the complicated interaction of interfering signal characteristics with receiver signal processing functions, IPC in general cannot be determined from analytic frequency dependent rejection (FDR) formulas [2], [3]. Consequently, engineers at the National Telecommunications

[1] The author is with the Institute for Telecommunication Sciences (ITS), National Telecommunications and Information Administration, U.S. Department of Commerce, Boulder, CO 80305.
[2] The author was formerly with the Institute for Telecommunication Sciences (ITS), National Telecommunications and Information Administration, U.S. Department of Commerce, Boulder, CO 80305.

and Information Administration (NTIA) Institute for Telecommunication Sciences (ITS) often estimate IPC with measurements of operational equipment in the laboratory or field.

These measurements are often hindered by equipment availability, which can be limited because the equipment:

- Has yet to be manufactured
- Was not manufactured in large numbers
- Cannot be removed from service for tests

Measurements are also hindered by inaccessible receiver:

- Operational parameters needed to control measurement conditions
- Performance metrics needed to quantify degradation
- Intermediate signals needed to determine vulnerable receiver subsystems

All of these factors can make accurate and repeatable measurements difficult to obtain by ITS and other interested parties.

The purpose of this research is to determine if radio system software simulation can accurately emulate these measurements and alleviate their hindrances. Our approach is to use the commercial off-the-shelf (COTS) radio system simulator software described in Appendix A to model previous IPC measurement test fixtures and compare measured IPC test results to simulated IPC test results.

Currently, there is considerable interest in Long Term Evolution (LTE) cellular radio systems sharing spectrum with Federal radars in the 3.5 GHz Citizen Broadband Radio System (CBRS) band [4], [5], and [6]. NTIA's Office of Spectrum Management (OSM) and ITS have conducted a number of IPC measurements, summarized in Table 1, with time division duplex (TDD) LTE, frequency division duplex (FDD) LTE, and pulsed radar for various cases of this sharing scenario. Consequently, we have chosen to emulate IPC measurements for SPN-43C radar interference in LTE/FDD user equipment (UE) receiver corresponding to Case 3 and LTE/FDD evolved node B (eNB) interference in a SPN-43C radar receiver corresponding to Case 4.

Table 1. NTIA OSM and ITS IPC Measurements. Shaded case results are compared to simulation results in this report. GN refers to Gaussian noise.

Case	**Receiver**	**Interfering signal**	**NTIA Report**
1	LTE/TDD eNB	GN, Pulsed	[7]
2	LTE/FDD eNB	GN, Pulsed	[8]
3	LTE/FDD UE	GN, Pulsed	[8]
4	SPN-43C	GN emulating LTE/FDD eNB	[9]
5	SPN-43C	LTE TDD eNB	[9]

This report is divided into scenario, LTE/FDD UE receiver IPC, SPN-43 radar receiver IPC, and conclusion sections. The scenario section contains a description of the interference environment and equipment. The IPC sections contain a description of the measurement and simulation methods and a comparison of measurement and simulation results.

2. GENERAL IPC TEST

Figure 1 is a block diagram of the general IPC test fixture. The desired signal is transmitted, subjected to the interfering signal, and received. Frequency separation between the desired and interfering signal carrier frequencies can be imposed by applying a frequency offset to the interfering signal. Both desired and interfering signals are degraded by independent propagation channels which are often only the attenuation needed to control their powers. Performance is quantified with metrics such as error rate, probability of detection, P_d, or probability of false alarm, P_{fa}.

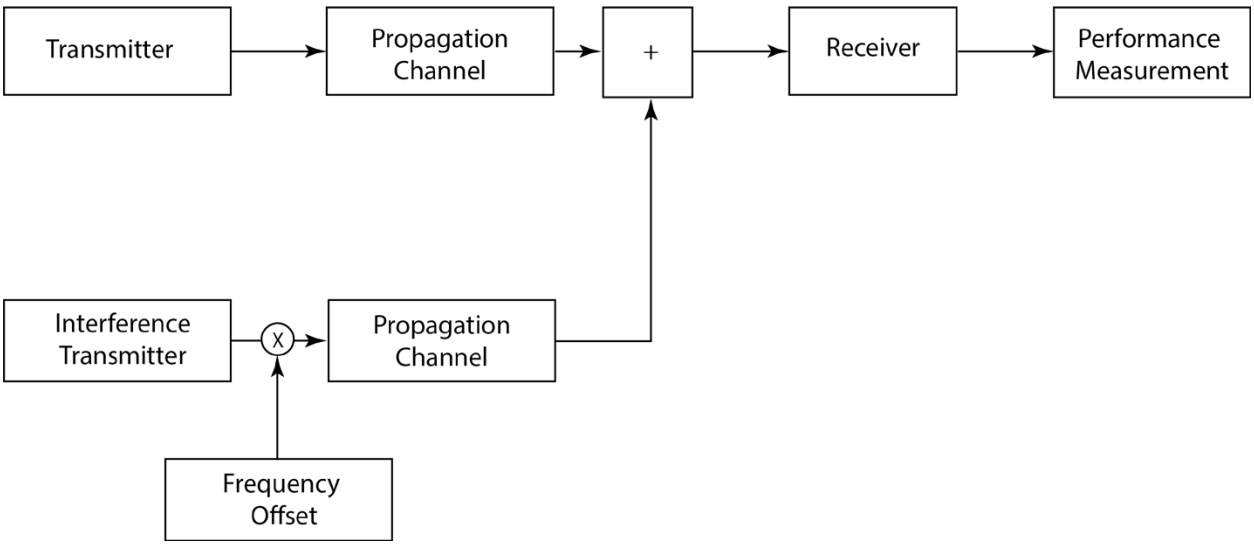

Figure 1. General IPC test fixture. The desired signal is transmitted, degraded by the propagation channel and interfering signal, and received. Desired and interfering signals go through independent propagation channels since their transmitters are generally not co-located.

Desired signal, interfering signal, and receiver noise are designated $s(t)$, $i(t)$, and $n(t)$, respectively. Corresponding powers are designated s, n, and i. Power in dB units is represented with capital letters and power in watt units is represented in lower case letters.

Powers are generally reported as average powers at the receive antenna output. Pulsed radar power is the average power of the pulse while "on," which is sometimes measured with a peak detector. Gaussian noise (GN) interfering signal power is the average power in the detection bandwidth. Receiver noise power is the average power in the detection bandwidth referred to the receive antenna output by the noise figure.

The relevant power ratios are signal power to noise power ratio

$$SNR = 10\log_{10}\left(\frac{s}{n}\right) = S - N, \tag{1}$$

interfering signal power to noise power ratio

$$INR = 10\log_{10}\left(\frac{i}{n}\right) = I - N, \tag{2}$$

and signal power to interfering signal power plus noise power ratio

$$SINR = 10\log_{10}\left(\frac{S}{i+n}\right). \tag{3}$$

The general IPC test method is

1) Set received signal power, S, to a baseline signal to noise ratio, SNR, corresponding to the nominal interference-free performance

2) Set interfering signal center frequency offset, Δf, to the lowest center frequency offset of interest

3) Set interfering signal power, I, to the lowest interfering signal power of interest

4) Measure performance

5) Increment interfering signal power and repeat steps 4 and 5 until highest interfering signal power is exceeded

6) Increment center frequency offset and repeat steps 3, 4, and 5 until highest center frequency offset is exceeded

Figure 2 shows how IPC test results at a single frequency offset are typically presented. The IPC are the allowed interfering signal power, I_a, or interfering signal power to noise power ratio, INR_a, corresponding to the allowed performance degradation, that have been identified by the spectrum sharing stakeholders after careful review of test results.

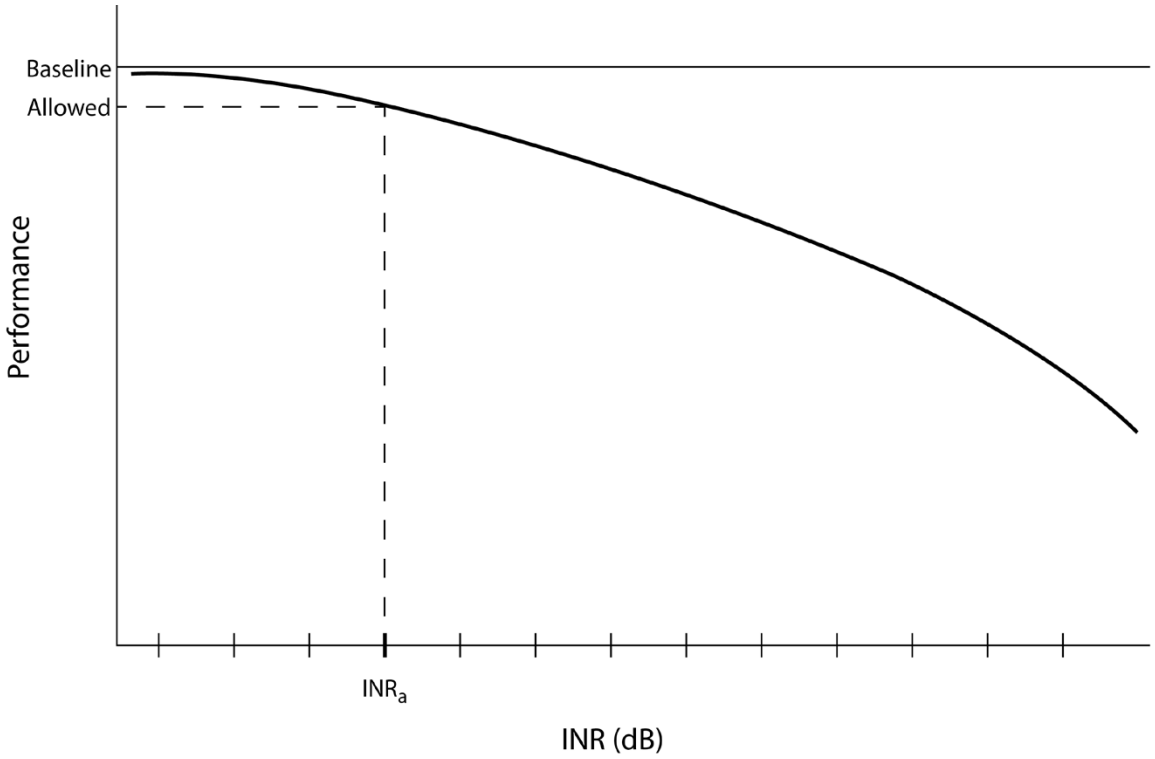

Figure 2. Graph showing how IPC test results at a specific frequency offset are typically presented. Baseline performance is evaluated without interference. The IPC is the allowed INR, INR_a, corresponding to the degraded allowed performance.

3. SCENARIO

The interference scenario depicted in Figure 3 shows an LTE/FDD eNB transmitting to an LTE/FDD UE over what is referred to as its downlink. At the same time the SPN-43C radar referred to as “Shipborne Radar 1” (SBR-1) in [4] is transmitting a signal whose received reflection determines the location of the target. Here we examine LTE eNB interference in the radar and radar interference in the LTE UE. Assumed LTE/FDD eNB and radar power spectral densities are depicted in Figure 4.

The IPC measurements emulated in this study impose the following restrictions on the scenario

- Signals are transmitted on the same carrier frequency with no frequency offset
- All propagation paths, including the path from the radar to the target, are free of frequency-selective and frequency-flat fading
- The radar targets are stationary with non-fluctuating, Swerling 0 radar cross sections (RCS)
- There are no radar clutter returns from precipitation, terrain, buildings, or vegetation
- The LTE/FDD eNB interfering signal is emulated by GN.

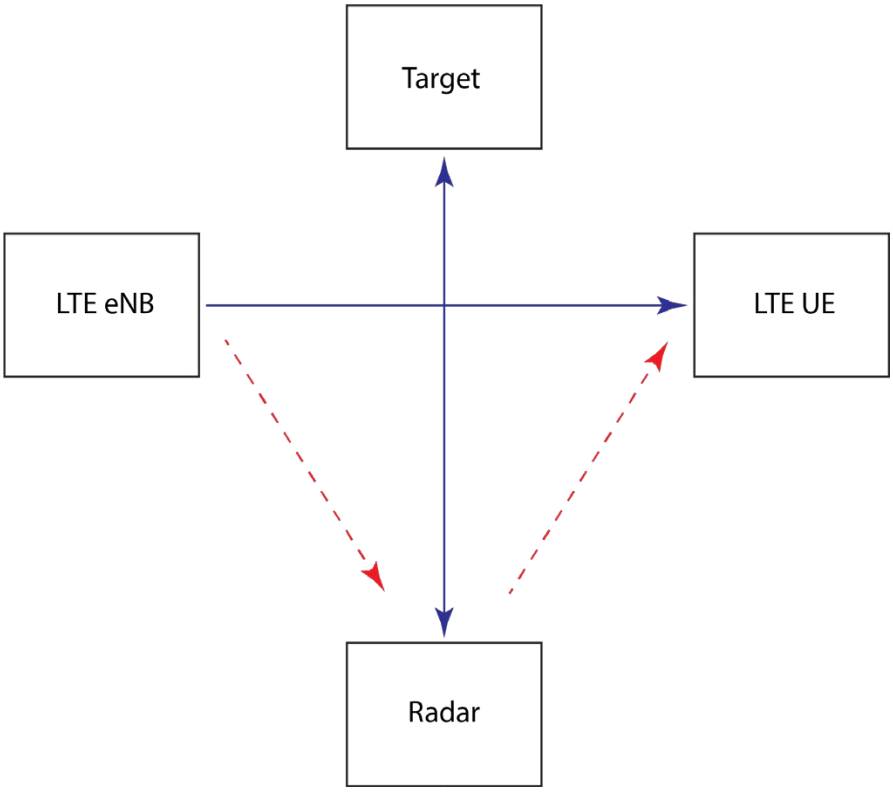

Figure 3. Interference Scenario. Blue lines indicate desired signals and red lines indicate interfering signals.

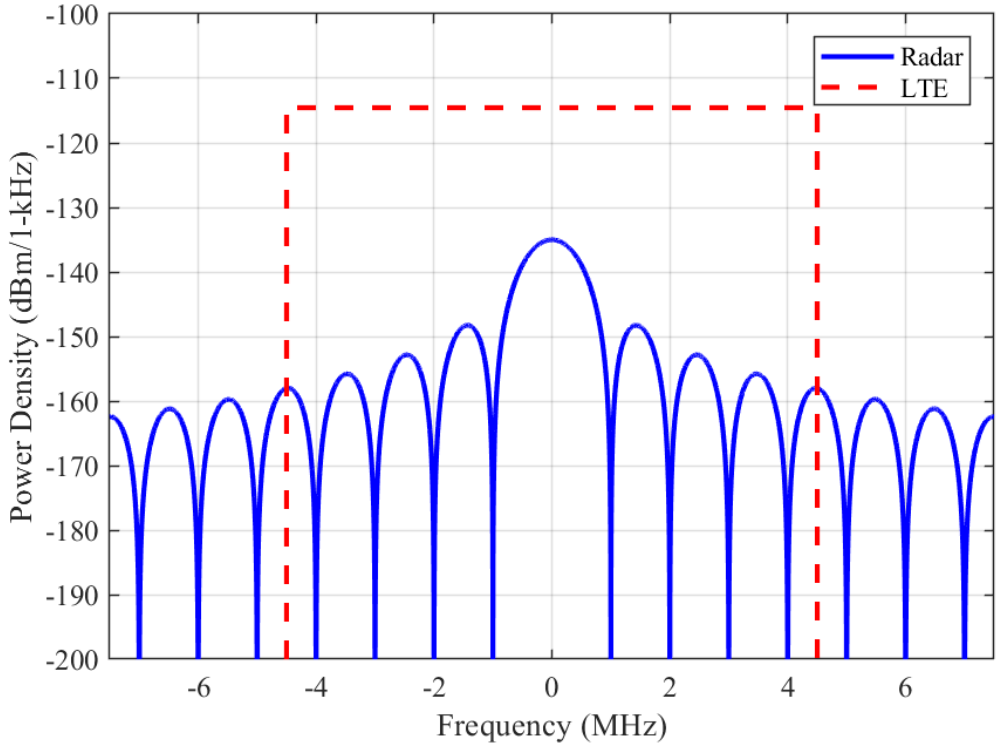

Figure 4. Ideal SPN-43C radar and LTE/FDD eNB power spectral densities for -75 dBm peak radar and average LTE powers.

3.1 LTE/FDD Downlink

LTE mobile radio systems represent a significant advance over earlier third generation (3G) mobile radio systems [10]–[13]. This section provides a brief overview of downlink signal structure and processing needed to understand the IPC measurement. More detailed information including a signal processing block diagram is provided in Appendix B.

The LTE/FDD downlink uses orthogonal frequency division multiple access (OFDMA) to send orthogonal frequency division modulated (OFDM) words from the LTE/FDD eNB to a number of UEs. The OFDM words are organized into 10 millisecond (ms) frames, 1 ms subframes, and 0.5 ms slots. OFDM word duration is 1⁄14 ms nominally but increases to 1⁄12 ms when the radio channel introduces long delays. The fundamental spectrum resource allocation unit is the 180 kHz wide, ½ ms long resource block (RB). Nominally, the RB is composed of 84 resource elements (RE) composed of 7 sets of 12 subcarriers spaced 15 kHz and one OFDM word duration apart.

Every 1 ms transmit time interval (TTI) the media access control (MAC) layer presents downlink information to the physical layer in discrete transport blocks (TB). The size of the TB is determined by modulation order, coding rate, and number of allocated resource block pairs. The information is organized into data channels, overhead channels, and overhead signals. The data channels are referred to as physical downlink shared channels (PDSCH). The overhead channels

include the physical downlink control channels (PDCCH) and the physical broadcast channels (PBCH). The overhead signals include the secondary synchronization signal (SSS), primary synchronization signal (PSS), and the common reference signal (CRS).

LTE uses link adaptation, hybrid automatic repeat request (HARQ) retransmission, and multiple antenna adaptation to mitigate attenuation, shadow fading, and multipath radio channel propagation effects. Conceivably these mechanisms could also mitigate interference so they are extremely important when accessing IPC.

Link adaptation, typically based on adaptive modulation and coding (AMC), matches the modulation and coding scheme (MCS) to radio channel conditions. The AMC function in the UE evaluates channel quality and reports the corresponding channel quality index (CQI) to the eNB. Channel quality is evaluated with metrics such as SNR and first transmission block error rate (BLER). The AMC function in the eNB assigns the downlink MCS corresponding to the CQI.

HARQ uses TB cyclic redundancy check (CRC) information to manage retransmissions. The UE calculates the TB CRC and reports to the eNB whether it is correct or not with an ACK or NACK signal, respectively. The NACK signal triggers a retransmission as long as the maximum number has not been exceeded.

HARQ is typically implemented with incremental redundancy. Incremental redundancy uses the highest coding rate (with the least redundancy) in the first transmission. Subsequent retransmissions use progressively lower coding rates (with more redundancy) and are “soft-combined” with previous transmissions before decoding.

Multiple antenna adaptation matches the multiple antenna rank and precoding matrix to radio channel conditions. Rank can be thought of as the number of independent data streams or “layers”. The precoding matrix distributes each layer’s modulated symbols across the available antenna “ports.” The UE measures each antenna port’s transfer function from which it determines the optimal rank and antenna port precoding matrix. The UE reports the corresponding rank index (RI) and precoding matric indicator (PMI) to the eNB.

3.2 SPN-43C Radar

The SPN-43C radar, designed and first operated in the 1960s, is a remarkably simple radar. As shown in Figure 5, the radar is composed of a rotating antenna, rotary joint, transmission line, circulator, transmitter, receiver, signal processor, data processor, and planned position indicator (PPI) display. The circulator passes signals from the transmitter to the antenna and from the antenna to the receiver.

The radar transmits a simple repetitive "on-off" carrier P0N[3] pulse train from a narrow beam antenna. When the pulse is not being transmitted the receiver listens for pulses reflected from aircraft in the sky.

Figure 6 shows a block diagram of the radar's signal processing functions implemented with an analog non-coherent integrator. The received pulses are envelope detected, non-coherently integrated to enhance SNR, and compared to a manually set threshold voltage. Additional signal processing consists of automatic gain control (AGC), sensitivity time control (STC) short range clutter mitigation, and fast time constant (FTC) precipitation clutter mitigation. While some SPN-43C radars have moving target indication (MTI) clutter rejection and constant false alarm rate (CFAR) automatic threshold setting signal processing functions, the radar that was measured did not have them.

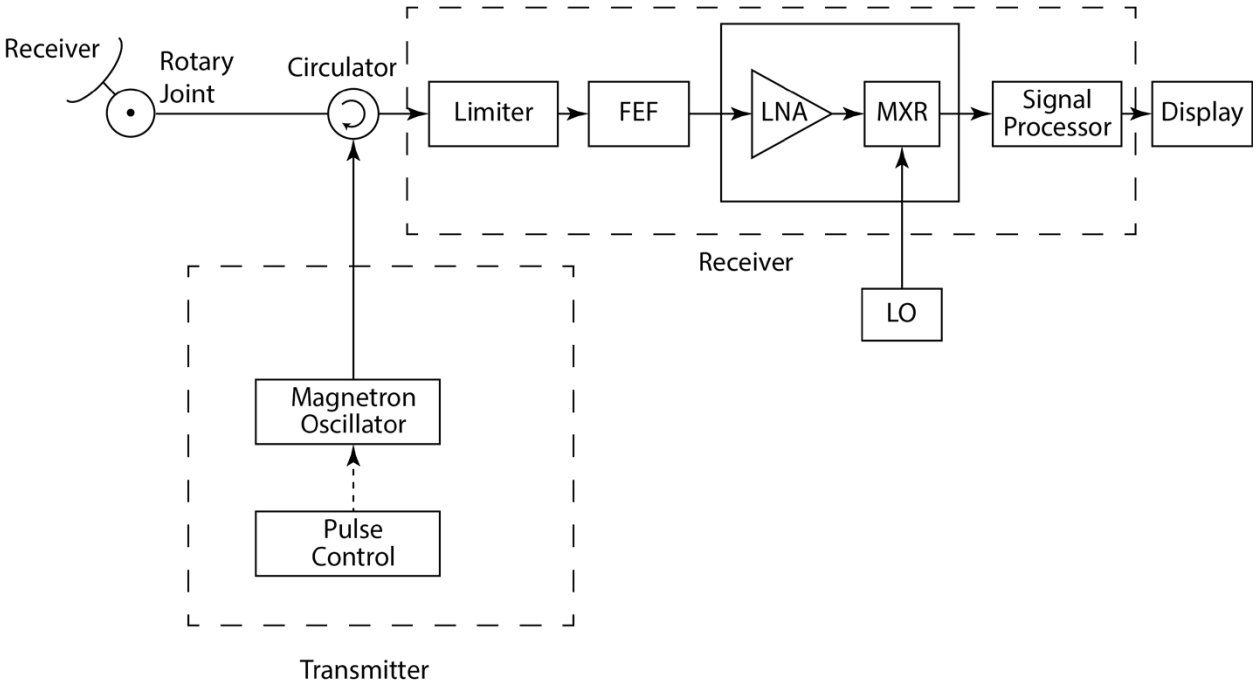

Figure 5. Block diagram of measured radar. FEF represents front end filter, LNA represents low noise amplifier, MXR represents mixer, and LO represents local oscillator.

[3] The P0N designation is used to identify this modulation in the *NTIA Manual of Regulations and Procedures for Federal Radio Frequency Management* (the NTIA "Redbook"), Section 9.8.2. http://www.ntia.doc.gov/page/2011/manual-regulations-and-procedures-federal-radio-frequency-management.

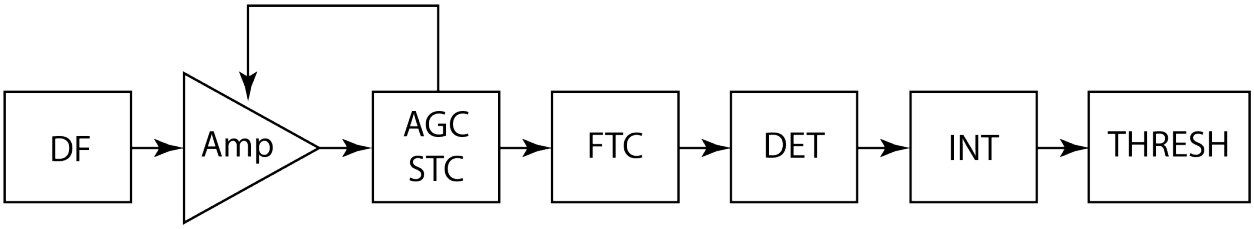

Figure 6 Block diagram of measured radar signal processor. DF represents detection filter, Amp represents amplifier, AGC represents automatic gain control, STC represents sensitivity time control, FTC represents fast time constant, DET represents detector, INT represents integrator, and THRESH represents threshold function.

4. LTE/FDD UE RECEIVER IPC

4.1 UE Receiver IPC Performance Metric

The LTE IPC measurements evaluated performance with throughput, BLER, and first transmission BLER metrics. The first transmission BLER metric ignores HARQ retransmission results. For FDD, throughput in bits per second, R_b, BLER, P_{block}, and first transmission BLER, $P_{block,first}$, are defined as

$$R_b = \frac{1}{NT_{sf}} \sum_{i=1}^{N} TBS_i \cdot \gamma_i \tag{4}$$

$$P_{block} = \frac{1}{N} \sum_{i=1}^{N} (1 - \gamma_i) \tag{5}$$

and

$$P_{block,first} = \frac{1}{\sum_{i=1}^{N} \chi_i} \sum_{i=1}^{N} (1 - \gamma_i)\chi_i \tag{6}$$

where N is the number of subframes transmitted (including retransmissions), T_{sf} is the 1 ms subframe period, TBS is the transport block size in bits, γ is the block cyclic redundancy check (CRC) (0/1 representing fail/pass), and χ is the first transmission indicator (0/1 representing retransmission/first transmission).

4.2 UE Receiver IPC Measurement

4.2.1 UE Receiver IPC Measurement Test Fixture

Figure 7 shows the UE receiver IPC measurement test fixture. The test fixture has two downlink paths from the eNB to the UE connected by cables and operating in rank-2, open-loop spatial-multiplexing transmission-mode (TM) 3. The uplink from the UE to the eNB needed to return CQI, RI, PMI, and HARQ ACK/NACK was implemented with a single cable and power splitter.

Two LTE traffic generators create the bits that the eNB converts to the downlink signal. Downlink interfering signals are added with two vector signal generators. While two interfering signal generators are redundant for the SPN-43C radar interfering signals, they are necessary for the GN interfering signals. Interfering signals are not applied to the uplink.

AMC, HARQ retransmission, and multiple antenna adaptation were used. However, details on their signal processing methods were not made available.

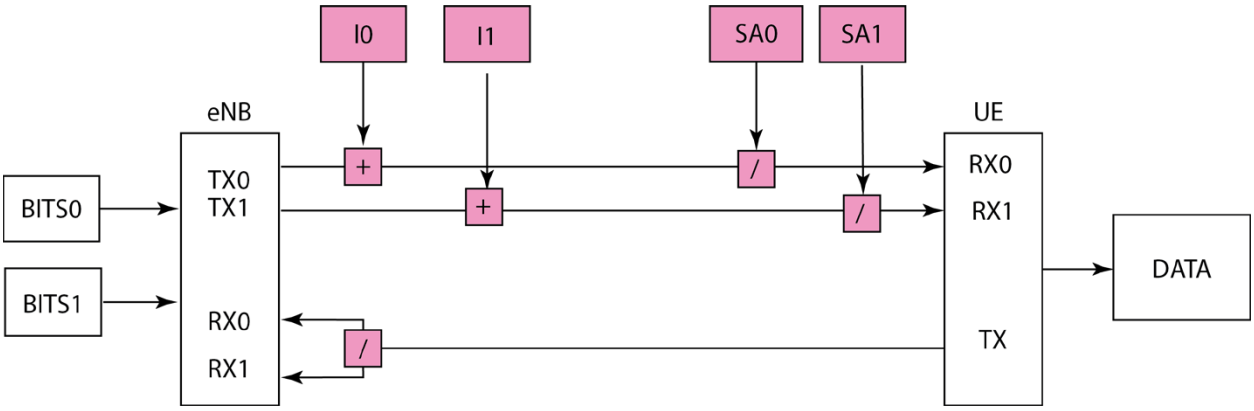

Figure 7. LTE IPC measurement test fixture. Shaded blocks represent test components and equipment. The two paths are designated by suffixes 0 and 1. BITS0 and BITS1 are the two LTE traffic generators, I0 and I1 are the two interfering signal generators, and SA0 and SA1 are the two spectrum analyzers for measuring signal and interfering signal powers.

4.2.2 UE Receiver IPC Measurement Method

Performance degradation measurements began after parameters were initialized and baseline SNR was established. While total signal power was measured, detailed information on how that power was distributed across data and overhead channels and signals was not known. At each interfering signal power, UE throughput, BLER, RI, MCS, and received signal strength indicator (RSSI) data was collected for 60 to 120 seconds.

Post measurement processing computed the mean and standard deviation of 100 throughput samples; mean and standard deviation of 2000 first transmission BLER samples; the minimum, mode, and maximum of an unspecified number of MCS samples in each rank; and the percent of time spent in each rank.

Because the SPN-43C pulse repetition interval (PRI) was the same as the LTE subframe period, the SPN-43C radar pulse is repeatedly placed on the same channel or signal as in Figure 8. The OFDM word the pulse was placed on was not documented in these measurements. However, if interference was not found at high interfering signal powers, engineers assumed the pulse fell on an empty OFDM word and the measurement was repeated.

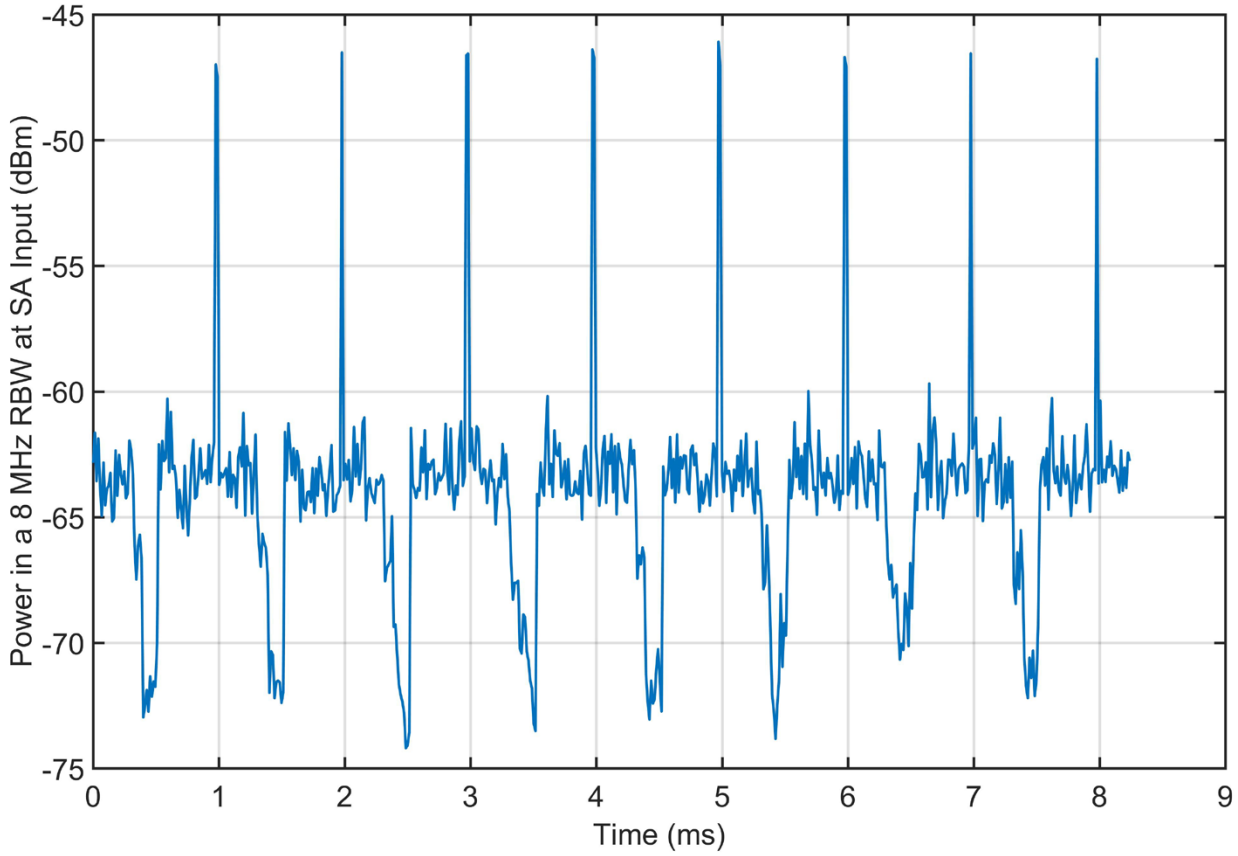

Figure 8. 10 MHz wide LTE/FDD waveform measured with a spectrum analyzer (SA) in an 8 MHz resolution bandwidth. Radar pulses occur every ms starting at one ms. LTE subframes, which also occur every ms, begin just before the periodic signal power drops. The drops are created by empty second and third PDCCH symbols.

4.3 UE Receiver IPC Simulation

4.3.1 UE Receiver IPC Simulation Model

Figure 9 is a block diagram of the IPC simulation model. The model has two downlink paths from the eNB to the UE and operates in open-loop spatial-multiplexing TM 3. The uplink is replaced with dedicated HARQ CRC and CQI feedback lines. Two LTE traffic generators create the bits the eNB converts to the downlink signal. Downlink interference is added with two signal generators.

As shown in Table 2, the simulation model set the RE power ratios to 0 dB with the exception of the PSS and SSS power ratios which were 10 dB. The AMC estimated SNR from the PSS. CQI was based solely on the estimated SNR. Appendix C describes how the AMC SNR/CQI/MCS conversion table was created. Multi-antenna adaptation was not available in the simulation model. However, since the measured equipment multi-antenna adaptation spent almost all its time in rank 2, the simulation model could be fixed at rank 2.

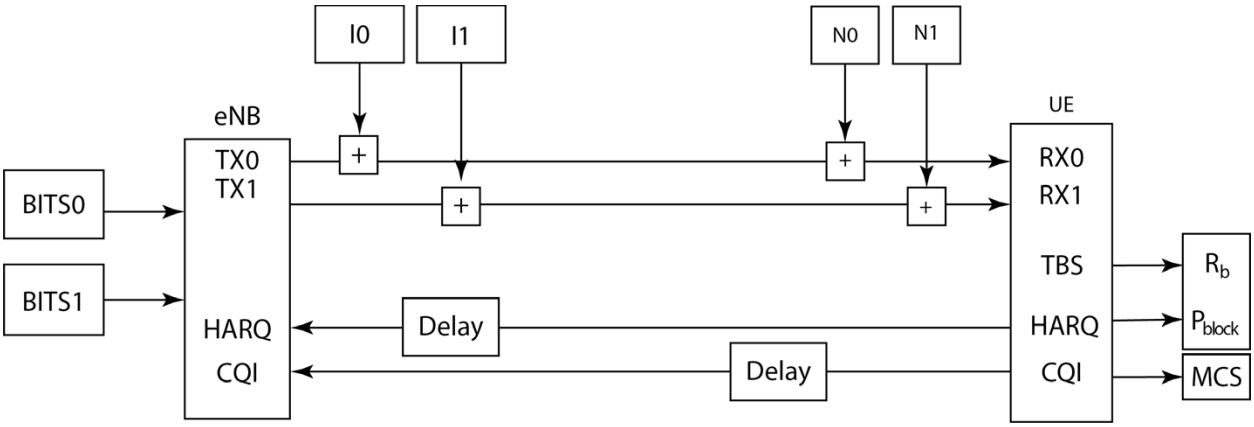

Figure 9. LTE IPC simulation model. I0 and I1 are independent interfering signal generators. N0 and N1 are independent receiver noise generators. TBS and HARQ CRC are used to calculate R_b and P_{block} . HARQ CRC and AMC CQI information are fed back to the eNB over dedicated lines.

Table 2. Simulation RE power relative to CRS RE power. Ra/Rb corresponds to power ratio for OFDM symbol with CRS/without CRS. CRS RE power is -25 dBm.

Parameter	**Simulation**	**Note**
PDCCH Ra/Rb	0/0 dB	
PHICH Ra/Rb	0/0 dB	
PBCH Ra/Rb	0/0 dB	
PCFICH Rb	0 dB	
PSS Ra	10 dB	
SSS Ra	10 dB	
P_A	0 dB	PDSCH RE power ratio for OFDM words without CRS
P_B	0 dB	PDSCH RE power ratio for OFDM words with CRS
P_B /P_A	1	

4.3.2 UE Receiver IPC Simulation Method

Simulations began after parameters were initialized and baseline SNR was established. At each interfering signal power, 1000 TBs were transmitted and received, and throughput, BLER, final CQI, and TBS were determined. Final MCS was inferred from the final CQI. The simulation was done two times. The first time with HARQ disabled to obtain first transmission metrics. The second time with HARQ enabled to obtain metrics after any necessary retransmissions.

SPN-43C interference simulations repeatedly placed pulses on the first, fourth, fifth, sixth, and seventh OFDM words of the subframe interfering with PDCCH, PDSCH, SSS, PSS, and PBCH respectively.

4.4 Comparison of UE Receiver IPC Operational Parameters

Tables 3 compares measurement and simulation operational parameters. Table 4 compares baseline conditions.

Table 3. Operational parameter comparison.

Parameter	Measurement	Simulation	Comparison	Note
eNB transmit antennas	2	2	Same	
UE receive antennas	2	2	Same	
Transmission mode	3	3	Same	Open loop spatial multiplexing
LTE channel allocation	10 MHz	10 MHz	Same	
Number of RBs	50	50	Same	
Signal bandwidth	9 MHz	9 MHz	Same	
Maximum MCS	23	27	Different	The simulation was capable of higher MCS than the measured equipment so it was used.
Maximum TBS	51,024 bits	63.408bits	Different	50 RB, 2 layers Table 7.1.7.2.1 in [13]
Maximum throughput	51.024 Mbps	63.408 Mbps	Different	
UE noise figure	7 dB	7 dB	Same	
Cyclic Prefix	Normal	Normal	Same	
RB mapping type	Localized	Localized	Same	
Number of PDCCH symbols	3	3	Same	
Number of antennas PSS/SSS is transmitted on	Unknown	1	Unknown	
CSI-RS	Disabled	Disabled	Same	
UE turbo code iterations	Unknown	8	Unknown	
AMC	Enabled	Enabled	Same	
AMC SNR estimation	Unknown	PSS	Unknown	Measured presumed to be CRS based
HARQ	Enabled	Enabled	Same	
Maximum HARQ retransmissions	8	8	Same	
RV sequence	[0,2,3,1]	[0,2,3,1]	Same	Redundancy Vector (RV)
UE category	2	2	Same	Category 2 has 1,237,248 soft memory bits
Rank Adaptation	Enabled	Not Available	Different	
Number of Ranks	2	2	Same	

Table 4. UE receiver IPC baseline condition parameters.

Parameter	Measurement	Simulation	Comparison	Note
Received signal power	-75 dBm	-75 dBm	Same	
UE Noise floor	-97.5 dBm	-97.5 dBm	Same	9 MHz bandwidth, 7 dB noise figure
Baseline received SNR	22.5 dB	22.5 dB	Same	
Baseline throughput	48.0 Mbps	63.408 Mbps	Different	

4.5 Comparison of UE Receiver IPC Results

Measurement and simulation throughput, first transmission BLER, and MCS results were compared for GN and SPN-43C radar interference. Simulated MCS is the final MCS while measured MCS is the mode of many transmissions.

While not immediately relevant to the interference scenario, GN interference results provide another way to evaluate simulation model fidelity. GN interference throughput, first transmission BLER, and MCS are compared in Figures 10 and 11.

Measured and simulated results both show throughput gradually decreasing with increasing interfering signal power. Closer inspection reveals that the simulation tolerated more interfering signal power than the measurements for the same throughput. From -93 dBm to -87 dBm this difference is 6 dB. From -84 dBm to -69 dBm the difference decreases to 3 dB.

Simulated first transmission BLER is near zero while measured first transmission BLER is closer to the 0.1 target. This disparity could be caused by different AMC algorithms. The simulated AMC algorithm is based solely on estimated SNR. The measured equipment AMC algorithm is not known but these results suggest it may take first transmission BLER into consideration.

Despite these differences in throughput and BLER, MCSs are comparable over the entire interfering signal power range.

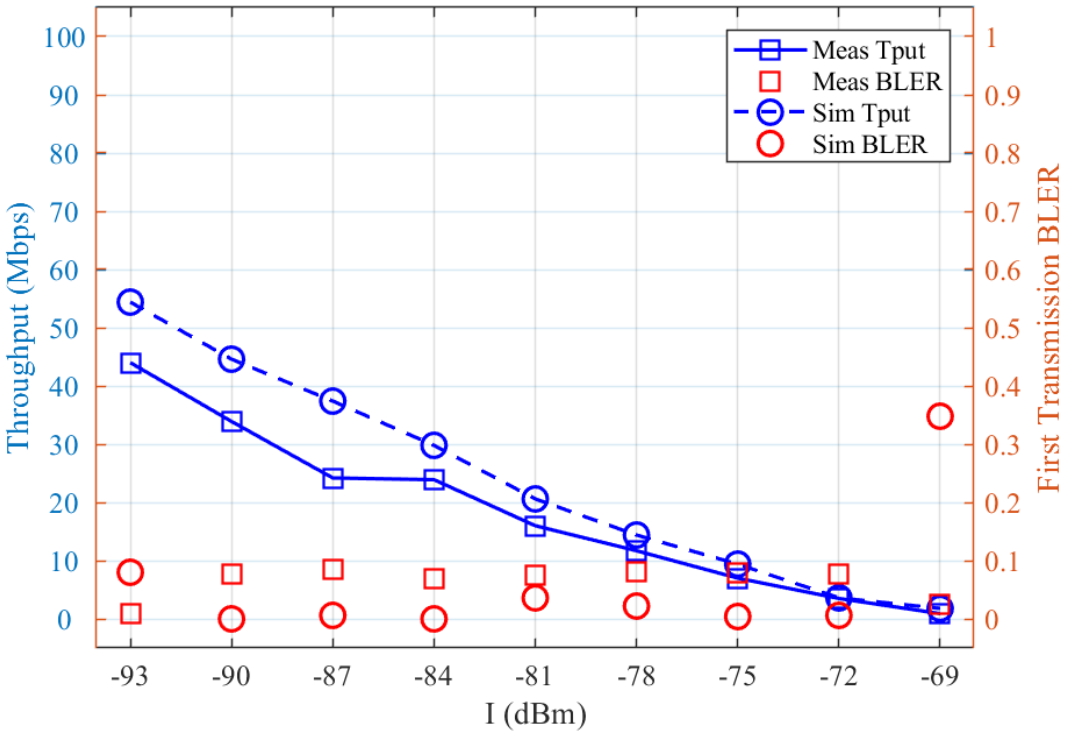

Figure 10. Comparison of measured and simulated throughput and first transmission BLER for GN interfering signal.

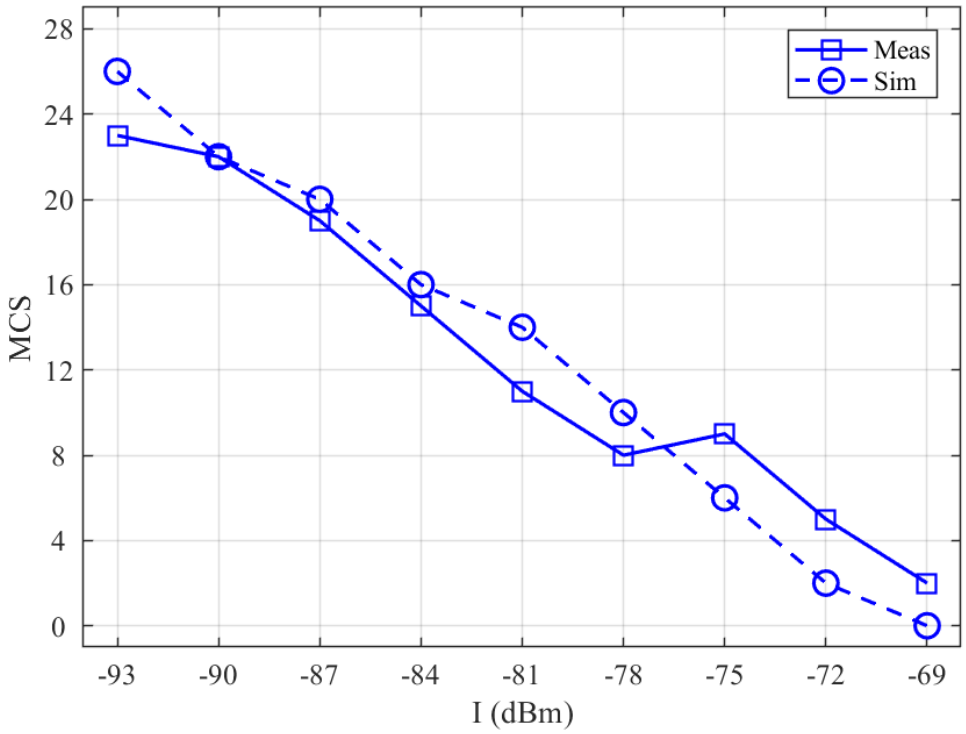

Figure 11. Comparison of measured and simulated MCS for a GN interfering signal.

SPN-43C radar interference results are compared in Figures 12-14. The measurements showed that as interfering signal power increased, throughput gradually decreased to a diminished but still useful rate. In fact, at -25 dBm, throughput is still approximately ⅓ of its maximum. First transmission BLER is near the 0.1 target. While the measured MCS degraded sharply at lower interfering signal powers, its degradation slowed considerably at higher interfering signal powers.

Simulated responses to the SPN-43C radar pulses fell into two categories. In the first category, when the pulse was repeatedly placed on the PSS, as interfering signal power increased throughput steadily degraded and was insignificant by -55 dBm. First transmission BLER was near 0 on all but the highest interfering signal power.

In the second category, when the pulse was repeatedly placed on the remaining OFDM words, throughput steadily degraded until -70 to -65 dBm, remained somewhat constant until -50 to -45 dBm, then completely stopped by -45 to -40 dBm. First transmission BLER was near 1 on all but the lowest interfering signal powers.

Differences between simulated results are best explained by the use of the PSS to estimate SNR for AMC. When the pulses are placed on the PSS and interfering signal power increases, the SNR degrades, and MCS decreases. Because the MCS is matched to radio channel conditions, first transmission BLER is near zero and few HARQ retransmissions are needed. In this case decreasing throughput is caused by the decreasing MCS.

However, when the pulses are placed in the remaining positions and interfering signal power increases, SNR and MCS stay the same. Because the MCS is so poorly matched to the radio channel conditions, first transmission BLER is 1.0 and HARQ retransmissions are needed. In this case decreasing throughput is caused by the increasing number of HARQ retransmissions.

In general, the measurement agrees most with simulations in the second category. However, it appears as though the measured equipment AMC function is able to assign a more viable MCS at higher interfering signal powers. First transmission BLER results suggest it may take first transmission BLER into consideration when assigning CQI.

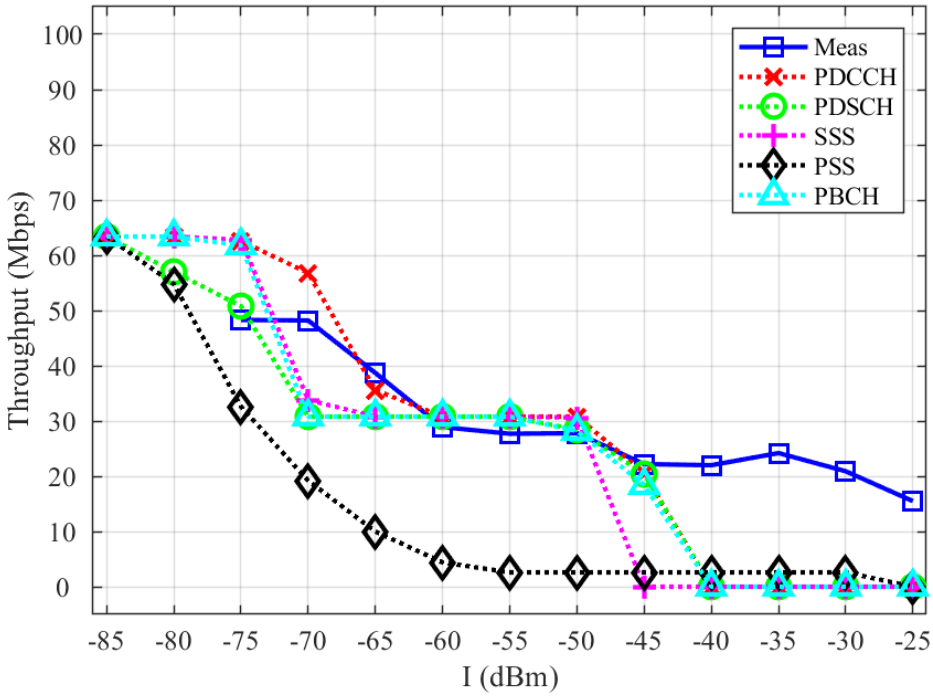

Figure 12. Comparison of measured and simulated PDSCH throughput with SPN-43C radar interference. Simulations placed pulses on OFDM words with the PDCCH, PDSCH, SSS, PSS, and PBCH.

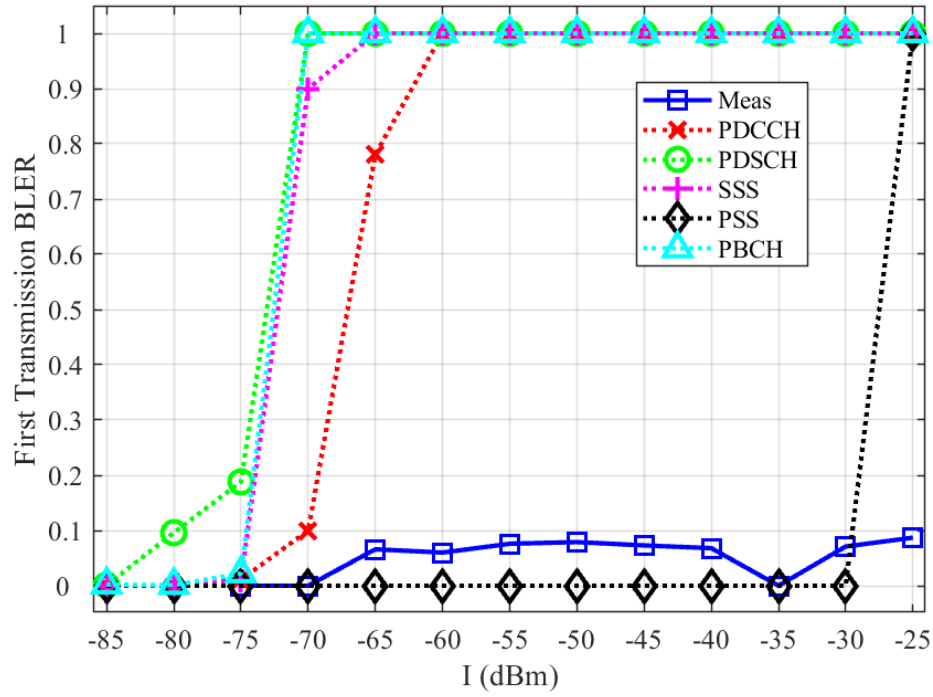

Figure 13 Comparison of measured and simulated first transmission BLER for SPN-43C radar interference. Simulations placed pulses on OFDM words with the PDCCH, PDSCH, SSS, PSS, and PBCH.

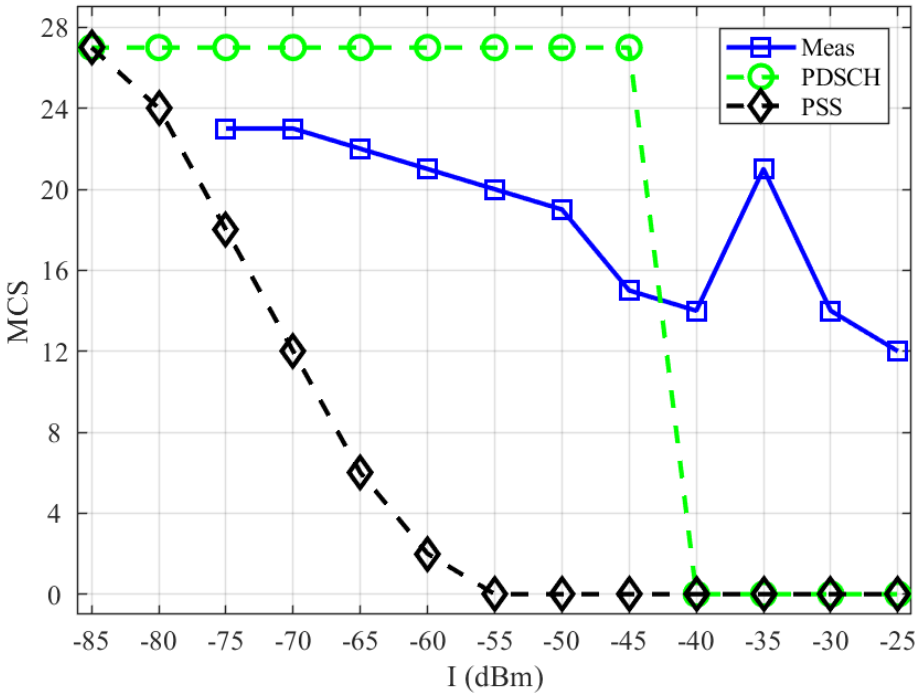

Figure 14. Comparison of measured and simulated MCS for SPN-43C radar interference. For clarity results from simulations that placed pulses on OFDM words with the PDCCH, SSS, and PBCH are not shown because they behaved almost identically to when pulses were placed on PDSCH.

5. SPN-43C RADAR RECEIVER IPC

5.1 Radar Receiver Performance Metric

Radar IPC measurements use probability of detection, P_d, and when possible, probability of false alarm, P_{fa}, to measure performance. Detection events can be characterized by

$$\gamma_{d,n} = \begin{cases} 1, f(s(t) + n(t) + i(t))|_{t=t_n} \geq d_t \\ 0, f(s(t) + n(t) + i(t))|_{t=t_n} < d_t \end{cases} \quad (7)$$

and

$$P_d = \frac{1}{N} \sum_{n=1}^{N} \gamma_{d,n} \quad (8)$$

where $f(\cdot)$ represents the signal processing steps needed to produce the decision statistic, N is the total number of trials and d_t is the detection threshold. Similarly the false alarm events can be characterized as

$$\gamma_{fa,n} = \begin{cases} 1, f(n(t) + i(t))|_{t=t_n} \geq d_t \\ 0, f(n(t) + i(t))|_{t=t_n} < d_t \end{cases} \quad (9)$$

and

$$P_{fa} = \frac{1}{N} \sum_{n=1}^{N} \gamma_{fa,n} \quad (10)$$

5.2 Radar Receiver IPC Measurement

5.2.1 Radar Receiver IPC Measurement Setup

IPC measurements were performed with the test fixture shown in Figure 15. Simulated target returns and interfering signals are created by vector signal generators (VSG) and conductively coupled into the receiver. GN was used to emulate the LTE/FDD eNB signal. Radar AGC was enabled. However, since clutter was absent, STC and FTC were disabled.

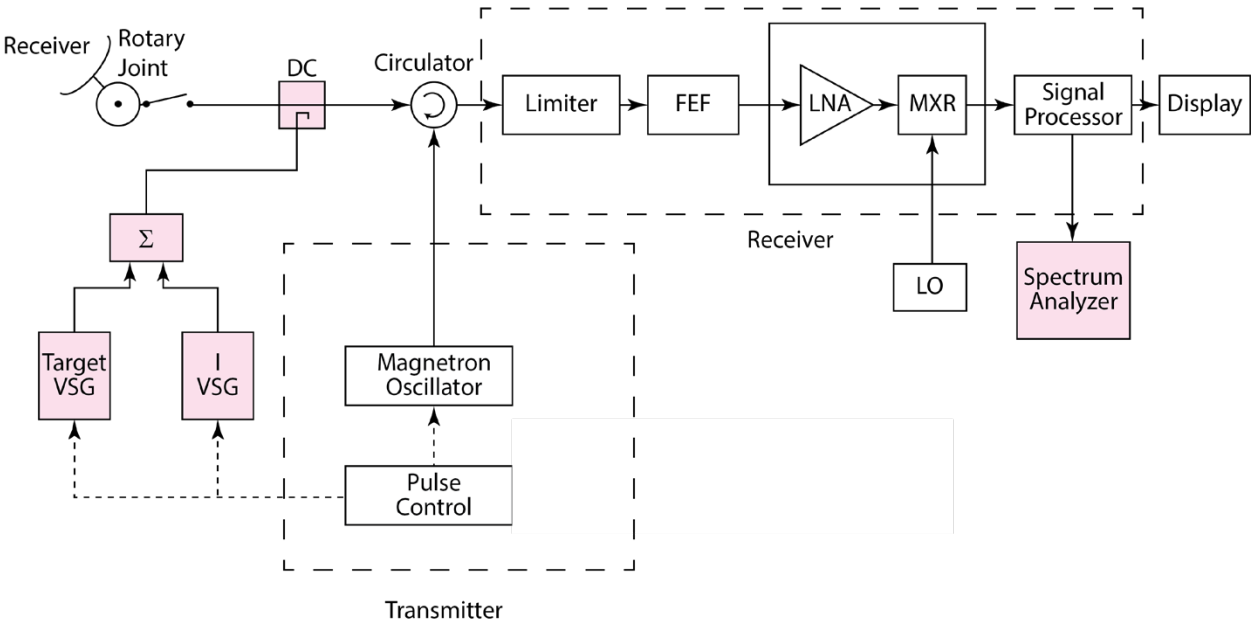

Figure 15. Block diagram of the SPN-43C radar measurement test fixture. Shaded blocks represent test components and equipment. DC represents directional coupler, Σ represents power combiner, FEF represents front end filter, LNA represents low noise amplifier, and MXR represents mixer.

5.2.2 Radar Receiver IPC Measurement Method

The SPN-43C IPC measurement was performed in the field at a radar test facility using a visual target counting method. This method was developed primarily because of difficulties encountered in the past using the radar's built in test equipment (BITE) function. In some cases operators trained in using the BITE function were not available. In other cases the radars did not have BITE functions [14].

The measurement begins by placing 10 stationary, non-fluctuating test target returns at evenly spaced ranges along a radar PPI display radial. Stationary targets make visual target identification easier. Non-fluctuating targets minimize the number of trials needed to obtain a satisfactory level of measurement uncertainty.

Test target returns at each range are repeated a number of times to emulate the arrival of pulses that are integrated in the time the radar beam sweeps through its 3 dB beam width. The pulses are equal in amplitude, emulating targets whose RCS increases with range to compensate for propagation loss.

P_d is estimated by counting the number of targets on the radar PPI display and dividing by the total number of targets sent. To execute the test, one engineer counts and announces the number of visible targets while another listens for the announcement and records the count in the laboratory notebook. The measurement is repeated if the counter thinks the count is in error. Typically, these measurements are made over 20 antenna rotation periods or scans for a total of 200 possible target detections at each interfering signal power.

The measurements begin in an interference-free baseline state where P_{fa} and P_d are set to the operator's preference. The P_{fa} was set by turning the interfering signal and target VSGs to the "RF off" state and adjusting the display gain control, i.e. the threshold, until the operator was satisfied with the number of false alarm "speckles." The target VSG was then set to the "RF on" state and its signal power was adjusted to produce a 0.9 P_d.

GN interfering signal power is calibrated relative to the system noise power by turning the target and interfering signal VSGs to the "RF off" state, measuring system noise power, turning the interfering signal VSG to the "RF on" state, and increasing interfering signal VSG power until the total power is 3 dB above the system noise power. At that point the interfering signal power is equal to the system noise power. The power measurement is executed with a spectrum analyzer in zero span mode in the radar detection bandwidth with RMS detection. The interfering signal generator center frequency is set to the radar's center frequency.

The interference is evaluated by iterating P_d measurements with incrementally increasing interfering signal powers. The interference is injected into the radar receiver at the same time the targets are injected. Between measurements the interfering signal is turned off for 10 antenna rotations to allow the radar to return to the baseline state. The next interfering signal power is then applied and the radar is allowed to adjust to the interfering signal for 10 antenna rotations. Hence, if 20 antenna rotation periods are used to count 200 targets, the entire measurement takes 40 antenna rotation periods.

It is important to note that no operator adjustments are made to compensate for the added interfering signal power. Most importantly, the engineer is not allowed to change the fixed threshold once the baseline false alarm rate is set.

5.3 Radar Receiver IPC Simulation

5.3.1 Radar Receiver IPC Simulation Model

Figure 16 depicts the radar simulation model block diagram. The model estimates all the parameters needed to establish IPC i.e. P_d, P_{fa}, S, N, and I. AGC, STC, and FTC were not implemented because the interfering signal did not overload the measured receiver and there was no clutter present. Figure 17 is a block diagram of the pulse integrator used.

On the P_d path, the transmitter generates a periodic pulsed signal. The signal is modulated by the RCS generator and receiver noise and interfering signal are added. The P_d is estimated by sampling the threshold output every PRI at the times the target is supposed to be present, summing the sampled sequence of ones and zeros, and dividing by the number of targets transmitted. The P_{fa} path operates on the composite noise and interfering signal. Other than not having a second sampler, its operation is identical to the P_{fa} path operation.

Signal, interfering signal, and noise powers are measured independently at the output of the detection filter. When the RCS is used to emulate a fluctuating target, the signal power must be averaged over a number of RCS realizations.

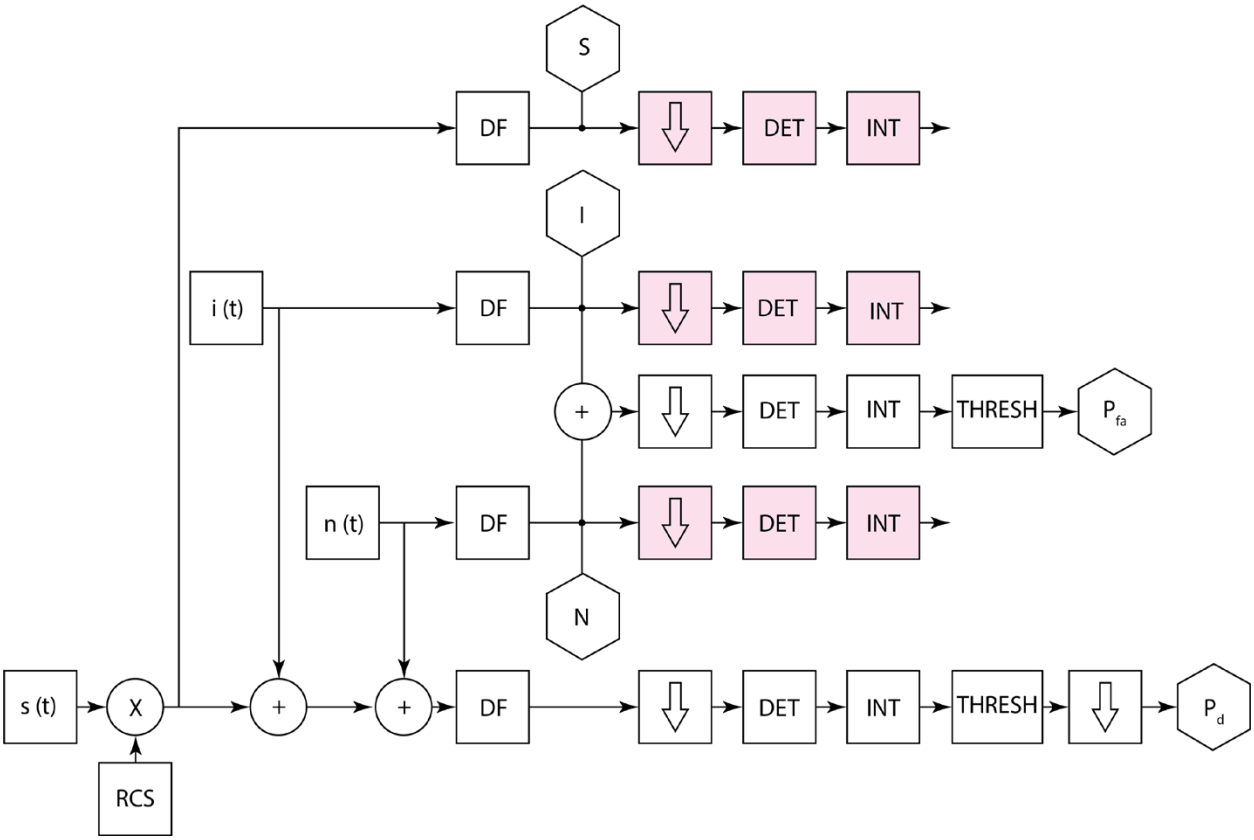

Figure 16. Block diagram of radar simulation model. RCS represents radar cross section, DF represents matched detection filter, down-arrow represents down-sampler, INT represents integrator, DET represents detector, THRESH represents thresholding function. Hexagonal blocks indicate measurements. Shaded blocks represent paths which enable the user to see isolated, signal-processed signal, interfering signal, and noise.

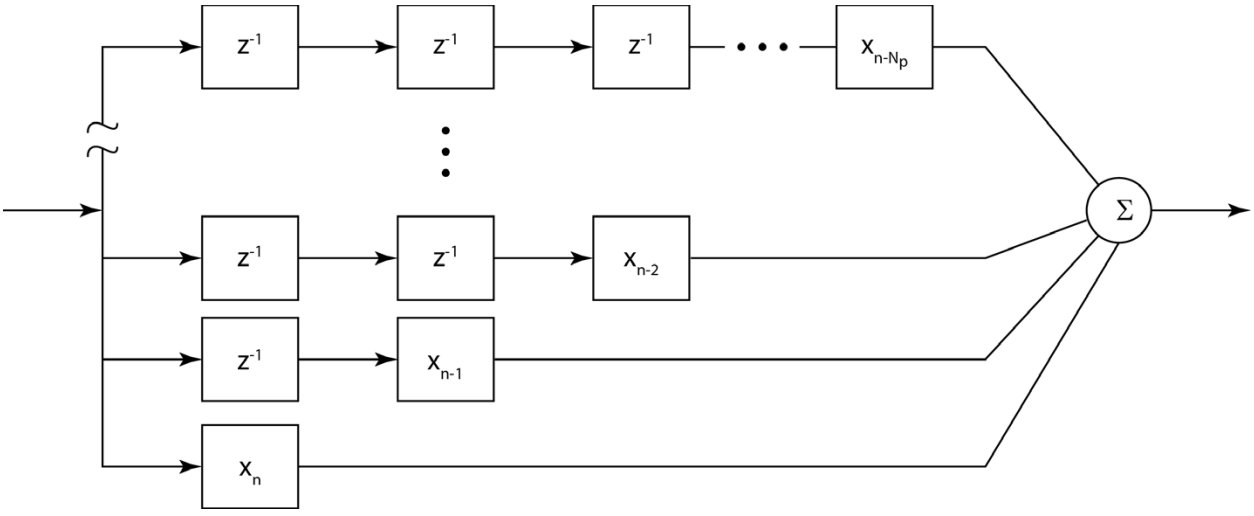

Figure 17. Block diagram of pulse integrator. The boxes with z^{-1} represent one PRI delay.

5.3.2 Radar Receiver IPC Simulation Method

Simulation execution time was minimized by eliminating antenna rotation dead time, minimizing the PRI, and determining the exact number of Monte Carlo trials needed. In normal surveillance radar operation, a narrow-beam antenna mounted on a rotating pedestal illuminates a point target for only a small fraction of the antenna rotation period. Simulation can completely eliminate antenna rotation dead time.

Furthermore in normal surveillance radar operation the PRI is set to correspond to the desired detection range. When simulating the effects of continuous interference on radars without CFAR the PRI can be reduced to the time it takes the pulse to decay. Finally, the exact number of Monte Carlo trials needed is determined by the desired P_{fa} uncertainty.

Threshold and baseline SNR settings were determined both analytically and through simulation. The practical fixed threshold for radars without CFAR is found by iterating threshold and measuring P_{fa}. The practical baseline SNR is then found by iterating SNR and measuring P_d.

Performance degradation simulations began after parameters were initialized and baseline SNR were established. At each interfering signal power, data was collected for the duration specified in Table 7. At the end of data collection, P_d, P_{fa}, S, N, and I were calculated.

5.4 Comparison of Radar Receiver IPC Operational Parameters

Table 5 compares operational IPC parameters.

Table 5. Radar receiver IPC operational parameter comparison. NA is not available.

Parameter	Measurement	Simulation	Comparison	Note
TRANSMITTED SIGNAL				
Modulation	P0N	P0N	Same	
Pulse width (μsec)	0.7	0.7	Same	Inverse of matched filter noise equivalent bandwidth
Pulse repetition frequency (Hz)	1000	1.42857×10^5	Different	
Pulse repetition interval	1.0 ms	7.0 μs	Different	
ANTENNA				
Antenna rotation period (sec)	3.8	NA	NA	
Antenna rotation rate (rpm)	15.6	NA	NA	
Azimuth beamwidth (deg)	1.9	NA	NA	
RECEIVED SIGNAL PROCESSING				
Integration	Non-coherent	Non-coherent	Same	
Threshold	Manual	Manual	Same	

Parameter	Measurement	Simulation	Comparison	Note
MTI	NA	NA	Same	
AGC	On	NA	Different	
STC	Off	NA	Same	
FTC	Off	NA	Same	
IF filter bandwidth (MHz)	1.4	1.4	Same	Equivalent noise bandwidths
Number of integrated pulses[4]	20	20	Same	

Table 6. Radar receiver IPC baseline condition parameters.

Parameter	Measurement	Simulation	Comparison	Note
P_d	0.9	0.9	Same	
P_{fa}	Unknown	10^{-5}	Unknown	
SNR	Unknown	2.6	Unknown	
Threshold	Unknown	12.8×10^{-12} V^2	Unknown	Simulation assumes a 0 dB noise figure

Table 7. Radar IPC execution parameters (per interfering signal power).

Parameter	Measurement	Simulation	Comparison	Note
Number of P_{fa} trials	Unknown	10^6	Unknown	
Number of P_d trials	200	10^5	Different	
Execution time (s)	150	120	Different	

5.5 Comparison of Radar Receiver IPC Results

Simulated results in Figure 18 show that P_d and P_{fa} increase with interfering signal power.[5] In contrast the measurements show P_d decreasing with interfering signal power. The stark difference between measured and simulated P_d results is most likely caused by differences in the meaning of detection. In the simulations a target is objectively detected if a voltage exceeds a threshold. In the measurements a target is subjectively "detected" if it can be visually discerned on the radar display. Simulation results show that the interfering signal is more likely to obscure a target with false alarms than cause it to disappear.

[4] The number of integrated pulses is determined by the number of pulses returned from a point target in the time it takes the antenna to rotate through its 3 dB beam width and is calculated by

$$n = \frac{\theta_B f_p}{6\omega_r}$$

where θ_B is the antenna 3 dB azimuthal beam width in degrees, f_p is the pulse repetition frequency in Hz, and ω_r is the antenna rotation rate in revolutions per minute (rpm).

[5] These results differ from those of radars with CFAR where P_d would decrease and P_{fa} would stay constant with increased GN interfering signal power.

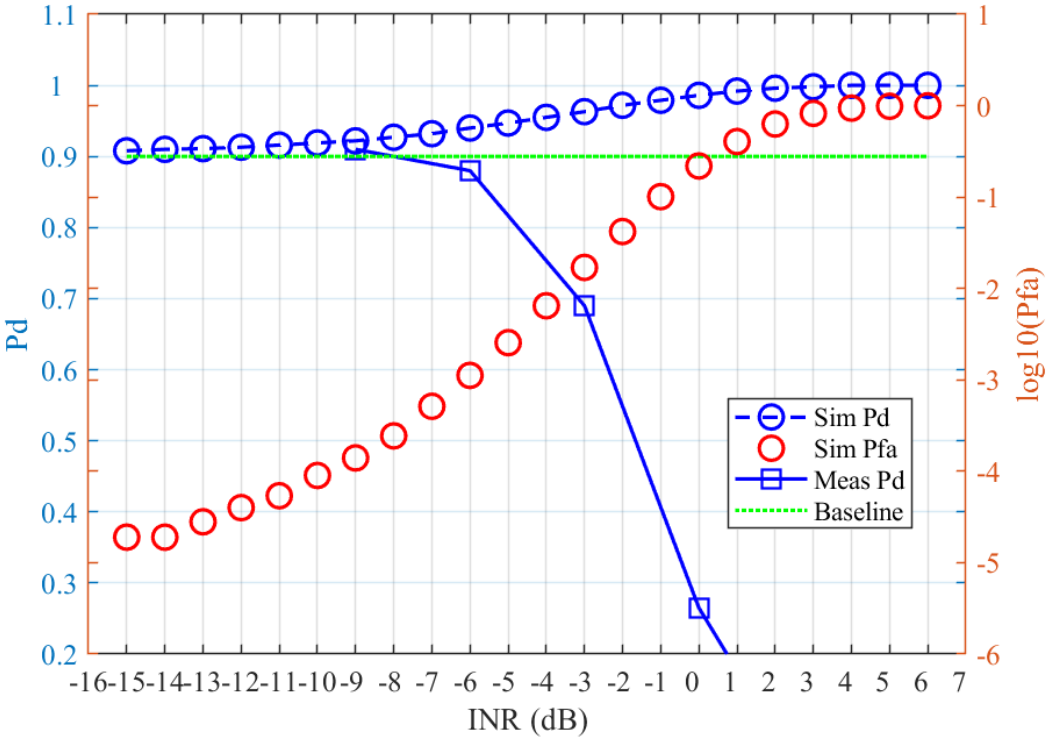

Figure 18. Simulated and measured results for SPN-43C radar with GN interfering signal.

This distinction is immediately evident from inspection of the PPI displays in Figures 19-22. Figure 19 is a photograph of the radar display under baseline conditions (without interference). The test targets are the 10 regularly spaced dots along the radial at 300 degrees azimuth. The speckles randomly scattered from 0 to 230 degrees are false alarms. The brightest wedge, attributed to prolonged camera exposure time, is not visible to the person counting targets during the measurement.

The baseline condition targets at the longer ranges towards the edge of the radar display are clearly visible and easily counted. However, even without interference, false alarms near the center of the display begin to compete for attention with the targets. Figures 20, 21, and 22 show how the targets become less distinguishable from the false alarms as interfering signal power increases from -6 dB INR to 0 dB INR. Ultimately, at 0dB INR, a bright, narrow beam or strobe completely obscures the targets we know are present since the threshold voltage has not changed.

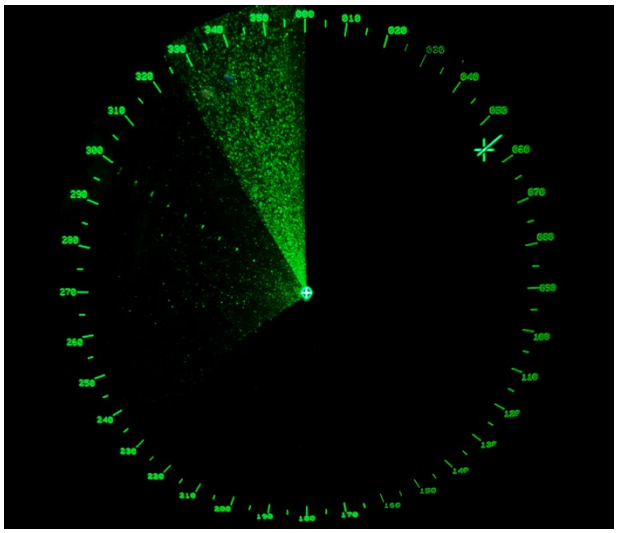

Figure 19. Baseline measurement with no interference. Estimated 0.885 P_d.

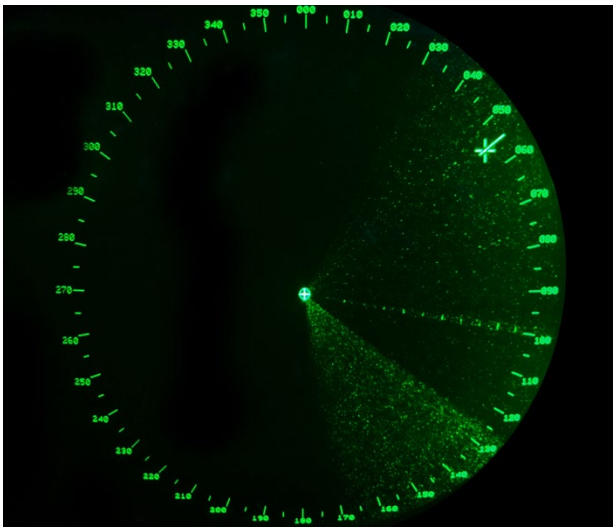

Figure 20. PPI display of -6 dB INR with GN interfering signal. Estimated 0.880 P_d.

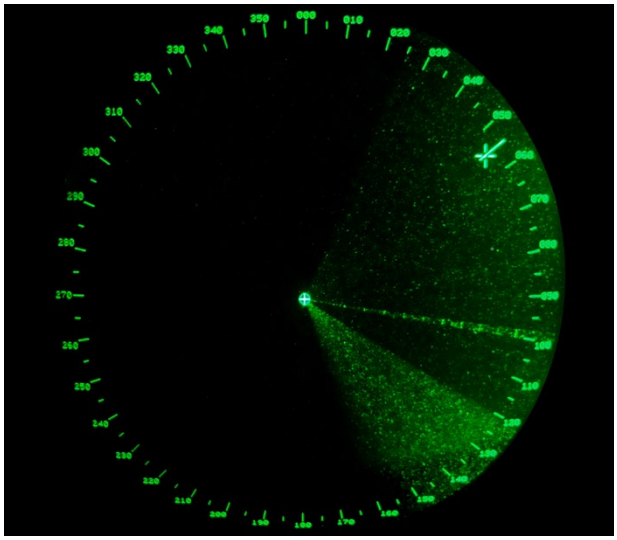

Figure 21. PPI display of -3 dB INR with GN interfering signal. Estimated 0.690 P_d.

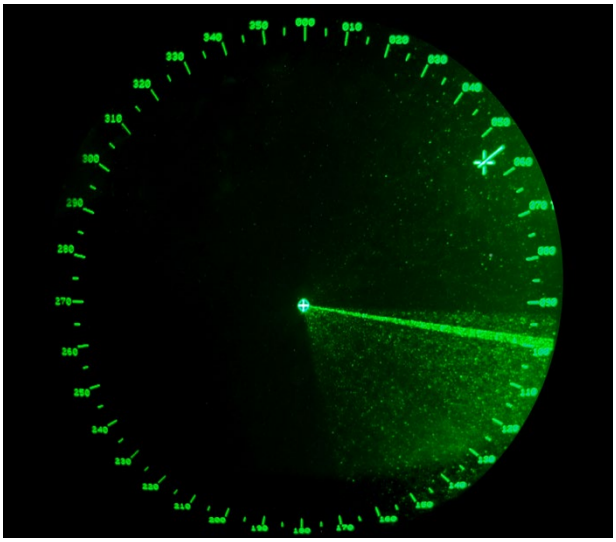

Figure 22. PPI display of 0 dB INR with GN interfering signal. Estimated 0.265 P_d.

6. CONCLUSIONS

The purpose of this research was to determine if radio system software simulation can accurately emulate IPC measurements executed in the laboratory or field and alleviate measurement hindrances such as lack of equipment availability and inaccessible intermediate signals or performance metrics. This conclusion summarizes our findings.

6.1 SPN-43C Radar Interference in LTE UE

The LTE equipment measured used AMC, HARQ retransmission, and multi-antenna adaptation to mitigate attenuation, shadow fading, and multipath radio channel propagation effects. Conceivably these mechanisms could also be beneficial for interference mitigation so it was imperative that the radio system simulation software include them. We found that the radio system simulation software did have AMC and HARQ retransmission but did not have multi-antenna adaptation. However since the measurement was conducted without multipath, multi-antenna adaptation was rarely executed by the equipment and its absence in the radio system simulation software did not cause a problem.

Simulated and measured GN interference throughput decreased with increased interfering signal power as expected. The decreased throughput was caused by decreased MCS which were roughly similar between simulation and measurement. However, there was an interfering signal power offset between the two for the same throughput and the measured equipment AMC was able to obtain a first transmission BLER nearer the 0.1 target. In spite of these differences we conclude that software simulation adequately emulated the GN interference measurement.

Because the SPN-43C PRI was the same as the LTE subframe period, the pulse was repeatedly placed on the same OFDM word within the LTE subframe. This allowed pulses to be placed repeatedly on the 3 channels (PDCCH, PDSCH, and PBCH) and 2 signals (SSS and PSS) within the LTE subframe. SPN-43C interference was measured for only one, unknown pulse placement.

Simulated results fell into two categories. Differences between results of these categories are best explained by the simulation AMC algorithm using the PSS to estimate SNR and ultimately assign MCS. In the first category, when the pulse was repeatedly placed on the PSS, as interfering signal power increased, throughput and MCS steadily decreased while first transmission BLER was zero. Clearly throughput degradation was caused by the MCS mitigating the interference.

In the second category, when the pulse was repeatedly placed on the other channels and signals, as interfering signal power increased throughput quickly degraded, remained somewhat constant, then completely stopped. At the same time MCS maintained its maximum level and first transmission BLER was 1.0. In this case throughput degradation was caused by HARQ retransmissions mitigating the interference.

Measured results showed throughput quickly degrading to approximately half its maximum then gradually degrading to one-third its maximum as interfering signal power increased. MCS degradation followed the same trend. First transmission BLER was near the 0.1 target.

In general, the measurement agrees most with simulations in the second category. However, it appears as though differences between the AMC functions allow the measured equipment AMC function to assign a more relevant MCS and continue operation at higher interfering signal powers. Better throughput might also have been made possible by a proprietary pulsed interference rejection (IR) algorithm [15] whose performance improved as the pulsed interference became stronger.

While there was significant agreement between the simulated and measured SPN-43C interference results, given the limited number of measured SPN-43C interference cases the agreement can only leave us with a hopeful optimism that software simulation can adequately emulate the SPN-43C IPC test. Measurements with more pulse positions and simulations with more sophisticated AMC are needed for a definitive conclusion.

6.2 LTE eNB Interference in SPN-43C Radar

Due to problems accessing the radar's BITE function, the IPC measurement used a visual target counting method. The radar's manually set fixed threshold, which was easily emulated by the radio system simulation software, significantly impacted this method's accuracy.

The simulation results showed that P_{fa} and P_d both increase with interfering signal power. These results are consistent with fixed threshold radars. Photographs of the measured radar PPI display clearly corroborated the P_{fa} increase with interfering signal power. However, in clear contrast to the simulation results, the measurement showed P_d decreasing with interfering signal power. This contradictory measurement result is most likely caused by targets being counted as missing when only obscured by false alarms.

Since the interference manifests itself primarily as false alarms, it is more appropriate to use the P_{fa} metric rather than P_d metric. Unfortunately P_{fa} is difficult to measure visually because the false alarms can occur anywhere on the radar display and are too numerous to count. Consequently software simulation is much better than measurements using the visual target counting method when IPC are needed for radars with fixed thresholds.

6.3 General

The radio system software simulator provided most but not all functions needed to accurately emulate the equipment and IPC measurement method. Notable deficiencies include the lack of a LTE multi-antenna adaption algorithm and AMC algorithm options. In this case, the lack of multi-antenna adaptation was not a problem because the measurement did not use time-varying multipath channels. However, it could be a problem in the future if regulators choose to conduct IPC tests under more "real-world" conditions. The profoundly different ways the simulated and measured MCS and first transmission BLER behaved with SPN-43C interference suggests their AMC functions operated differently. The simulated AMC estimated SNR from the PSS. There should also be options to estimate SNR from the CRS and take first transmission BLER into consideration when assigning CQI.

IPC measurements are often conducted as if the measured equipment is a “black box” operating under “nominal conditions.” In some cases, all that is known are the signal, noise, and interfering signal characteristics at its input and the performance metrics collected at its output. Details of equipment signal processing algorithms and parameter settings are left to the discretion of the equipment manufacturer. To some extent, this problem is due to the proprietary nature of the signal processing algorithms.

However, with software simulation, the scope of the IPC test must be enlarged by the necessary selection of receiver models and their associated signal processing algorithms and parameter settings. Ultimately, integration of software simulation into the spectrum engineering process and acceptance by the spectrum engineering community will depend on whether stakeholders find mutually-agreeable receiver models, algorithms, and parameter settings that can be feasibly implemented in today’s COTS radio system simulator software.

Overall, we found software simulation removed most measurement hindrances. Besides being readily available, the radio system software simulator provided almost unlimited access to the intermediate signals and performance metrics needed for IPC tests. These advantages can potentially enable engineers to identify vulnerable subsystems and recommend ways to make their operation more robust in the presence of the interfering signals.

With these considerations, we recommend more resources be devoted to the development of mutually agreeable receiver models so that IPC simulations can immediately supplement and someday replace IPC measurements.

7. REFERENCES

[1] A. Paul, G. Hurt, T. Sullivan, G. Patrick, R. Sole, L. Brunson, C.-W. Wang, B. Joiner, and E. Drocella, "Interference protection criteria," U.S. Dept. of Commerce, NTIA Report 05-432, October 2005, http://www.its.bldrdoc.gov/publications/2462.aspx.

[2] ITU Report 654-3, "Methods for Calculating Interference Power in Adjacent Bands and Channels," International Telecommunication Union, Geneva, Switzerland, 1990.

[3] ITU Report 972, "Peak Power Responses to Intermittent Interference Signals," International Telecommunication Union, Geneva, Switzerland, 1986.

[4] U.S. Dept. of Commerce, NTIA, "An Assessment of the Near-Term Viability of Accommodating Wireless Broadband Systems in the 1675-1710 MHz, 1755-1780 MHz, 3500-3650 MHz, and 4200-4220 MHz, 4380-4400 MHz Bands," Oct. 2010, https://www.ntia.doc.gov/report/2010/assessment-near-term-viability-accommodating-wireless-broadband-systems-1675-1710-mhz-17.

[5] FCC Further Notice of Proposed Rule Making, Proposes Creation of New Citizens Broadband Radio Service in 3.5 GHz, Federal Communications Commission, Washington D.C., USSA, FCC 14-49, GN docket no. 12-354, Apr. 2014.

[6] J.H. Reed, A.W. Clegg, A.V. Padaki, T. Yang, R. Nealy, C. Dietrich, C.R. Anderson, and D.M. Mearns, "On the Co-Existence of TD-LTE and Radar Over 3.5 GHz Band: An Experimental Study," *IEEE Wireless Communications Letters*, Vol. 5, No. 4, Aug. 2016, pp. 368-371.

[7] F. Sanders, J. Carroll, G. Sanders, and R. Sole, "Effects of Radar Interference on LTE Base Station Receiver Performance," U.S. Dept. of Commerce, NTIA Report 14-499, Dec. 2013, https://www.its.bldrdoc.gov/publications/2742.aspx.

[8] G. Sanders, J. Carroll, F. Sanders, R. Sole, "Effects of Radar Interference on LTE (FDD) eNodeB and UE Receiver Performance in the 3.5 GHz Band," U.S. Dept. of Commerce, NTIA Report 14-506, July 2014, https://www.its.bldrdoc.gov/publications/2759.aspx.

[9] F. Sanders, J. Carroll, G. Sanders, R. Sole, R. Achatz, L. Cohen, "EMC measurements for spectrum sharing between LTE signals and radar receivers," U.S. Dept. of Commerce, NTIA Report 14-507, July 2014, https://www.its.bldrdoc.gov/publications/2760.aspx.

[10] D. Astely, E. Dahlman, A. Furskar, Y. Jading, M. Lindstrom, and S. Parkvall, " LTE: The Evolution of Mobile Broadband," *IEEE Communications Magazine*, April 2009, pp. 44-51.

[11] ETSI TS 36.211, "LTE; Evolved Universal Terrestrial Radio Access (E-UTRA); Physical Channels and modulation," European Telecommunications Standards Institute, Sophia-Antipolis, France.

[12] ETSI TS 36.212, “LTE; Evolved Universal Terrestrial Radio Access (E-UTRA); Multiplexing and channel coding,” European Telecommunications Standards Institute, Sophia-Antipolis, France.

[13] ETSI ETSI TS 36.213, “LTE; Evolved Universal Terrestrial Radio Access (E-UTRA); Physical layer procedures”, European Telecommunications Standards Institute, Sophia-Antipolis, France.

[14] F. Sanders, R. Sole, B. Bedford, F. Pawlowitz, “Effects of RF Interference on Radar Receivers,” U.S. Dept. of Commerce, NTIA Technical Report TR-06-444, Feb. 2006. http://www.its.bldrdoc.gov/publications/2481.aspx

[15] H. Safavi, C. Ghosh, E. Visotsky, R. Ratasuk, and S. Roy, “Impact and Mitigation of Narrow-band Radar Interference in Down-link LTE,” in *Proc. of the IEEE ICC 2015 Wireless Communications Symposium*, pp. 2644-2649.

ACKNOWLEDGEMENTS

The authors would like to thank Ed Drocella, Chief of the Spectrum Engineering and Analysis Division, and Robert Sole, Chief of the Spectrum Engineering Branch, of the National Telecommunications and Information Administration (NTIA) Office of Spectrum Management (OSM) for their programmatic support.

The authors would also like to thank Frank Sanders, John Carroll, and Geoffrey Sanders of the NTIA Institute for Telecommunication Sciences (ITS) for their help in explaining IPC field measurement methods and results and Dr. Roger Dalke of the ITS for his consultation on various applied mathematics issues.

In addition, the authors would like to thank David Niday, Technical Support Engineer; Mark Knutson, Applications Engineer, Dingqing Lu, Scientist; and Jim Bau, Scientist, of Keysight EEsofEDA for their technical help with the radio system software simulator SystemVue.

Finally, the authors would also like to acknowledge Al Romero, Visual Information Specialist, of the National Oceanic and Atmospheric Administration (NOAA), for creating the illustrative figures.

APPENDIX A SIMULATION TOOL

Software simulations were performed with SystemVue radio system simulation software and a desktop computer. The software included the base RF-Architect algorithm design library, radar library, and LTE-A library [A-1], [A-2].

The user interacts with the software via a graphical user interface shown in Figure A-1. Data can be collected from any point in the diagram and analyzed during the simulation or after the simulation is complete. Although the software allows the user to create custom functions, the software came with most functions needed for this work.

The software was run on a desktop workstation with a 3.2 GHz Intel Xeon E3 processor, 8 megabytes of cache memory, 16 gigabytes of random access memory, and Windows 7 operating system.

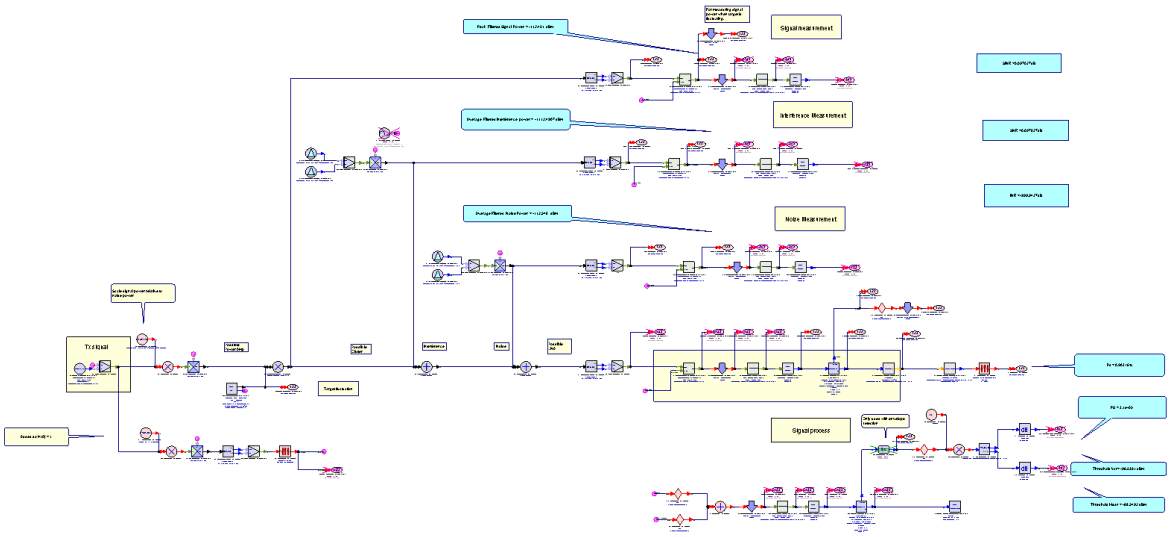

Figure A-1. Screen capture of radar model in radio system simulation software.

A.1 References

[A-1] Keysight Technologies, SystemVue Electronic System Level Design software, version 2016.08 released September 13, 2016.

[A-2] G. Jue, “Check for Co-Existence Between LTE and Radar,” *Microwaves & RF*, Dec. 2013, pp. 48-53.

APPENDIX B LTE DOWNLINK SIGNAL PROCESSING

B.1 Signal Composition

The downlink signal is composed of a number of physical layer channels and signals whose power can be set independently. The physical layer information bearing channel is referred to as the physical downlink shared data channel (PDSCH). Table B-1 lists a number of overhead channels and signals that are periodically multiplexed with the PDSCH. Figure B-1 shows their position in the first subframe.

Table B-1. LTE/FDD downlink overhead channels and signals.

Signal	Abbreviation	Function	Frame Position
Physical downlink control channel	PDCCH	Announces downlink control information (DCI) for uplink and downlink RB allocations	First 3 OFDMA symbols of subframe
Physical control format indicator channel	PCFICH	Announces number of PDCCH OFDMA symbols per subframe	First OFDMA symbol of subframe
HARQ indicator channel	PHICH	Returns HARQ CRC result to UE	First 3 OFDMA symbols of subframe
Primary synchronization signal	PSS	Channel time delay estimation	Last OFDMA symbol in first and eleventh slots of frame
Secondary synchronization signal	SSS	Channel time delay estimation	OFDMA symbol preceding PSS signal
Broadcast channel	PBCH	Announces eNB characteristics to UEs	First 4 OFDMA symbols in second slot of frame
Common reference signal	CRS	Data demodulation and channel state information reference	First, 5th, 8th, and 12th OFDMA symbol of subframe
Channel state information reference signal	CSI-RS	Channel state information reference	Depends on antenna port

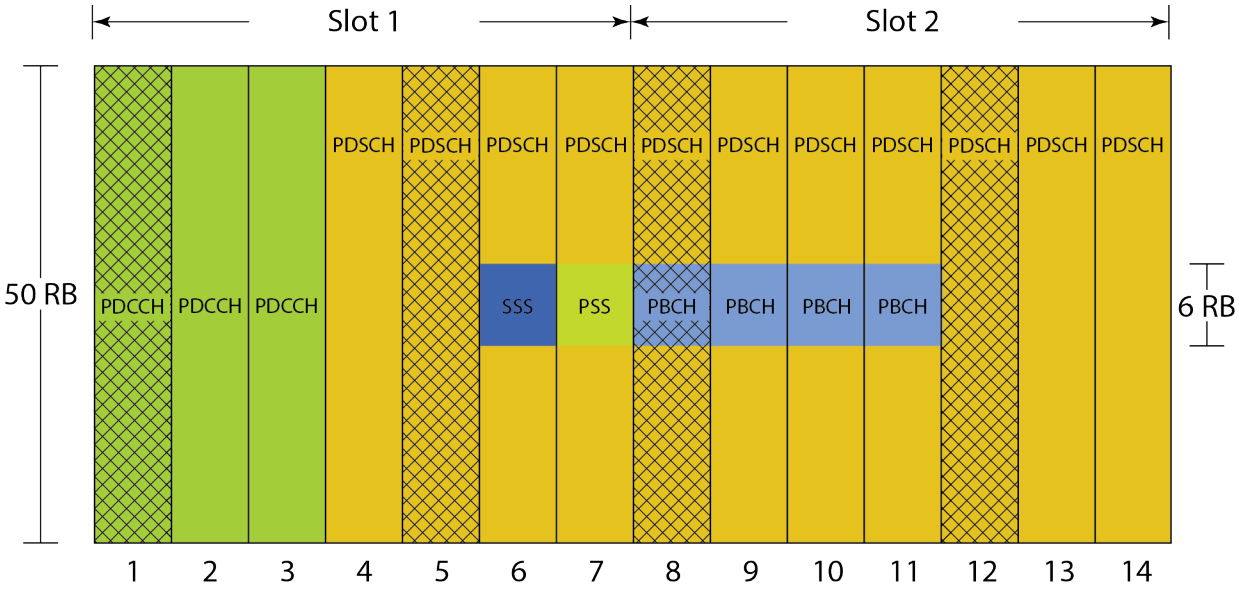

Figure B-1. Position of PDCCH, SSS, PSS, and PBSCH overhead channels in the first LTE FDD downlink signal subframe composed of 14 OFDM symbols. The signal bandwidth is 50 RB or 9 MHz. The SSS, PSS, and PBCH bandwidths are 6 RB or 1.08 MHz. OFDM symbols with CRSs are identified by crossing hatching. PCFICH and PHICH multiplexed with the PDCCH are not shown. PDCCH occur every subframe. SSS and PSS are spaced 5 subframes (one-half frame) apart. PBCH are spaced 10 subframes (1 frame) apart.

B.2 Signal Processing

The LTE signal processing steps of interest span the media access control (MAC) and physical (PHY) protocol layers. The MAC layer segments user data into variable sized transport blocks (TBs) for the PHY layer. Performance is quantified in terms of throughput and block error rate (BLER).

LTE signal processing is complicated by multiple antenna spatial multiplexing. To implement spatial multiplexing the transmitter must divide the modulated symbols into independent streams or layers that are mapped by a precoding matrix onto the transmit antenna ports. The number of spatial multiplexing layers is also referred to as the transmission rank.

Figure B-2 is a simplified depiction of the PDSCH signal processing operations [B-1], [B-2], and [B-3] for a single layer and single UE. Similar diagrams are available for the other signals in Table B-1. The top half represents the eNB transmitter signal processing and the bottom half represents the UE receiver signal processing. The UE receiver signal processing is fundamentally the inverse of the eNB transmitter. Additional processing estimates synchronization parameters, SNR, optimal rank, and optimal precoding matrix.

The CRC block computes and attaches a TB cyclic redundancy checksum (CRC). The code and rate matching (CRM) block segments the TB into one or more codewords (CW), computes and

attaches a CW CRC, and applies a forward error correction (FEC) code. The scrambler (SCR) block differentiates the signal from those of other eNBs

The modulator (MOD) block converts the scrambled bits to complex modulated symbols. The antenna mapper (AMAP) block divides the symbols into layers and applies the precoder matrix [B-4], [B-5]. The resource element mapper (RMAP) block maps the symbols to specific REs. The OFDM block applies an inverse Fourier transform. A portion of the transformed signal is repeated in the cyclical prefix (CP) to mitigate the effects of multipath.

The scheduler uses link adaptation typically implemented with adaptive modulation and coding (AMC), multiple antenna adaptation, and hybrid automatic repeat request (HARQ) to mitigate radio channel impairments and maximize spectrum efficiency. The scheduler accepts UE HARQ ACK/NACK and channel quality indictor (CQI) feedback to control the CRM and MOD blocks and UE rank index (RI) and precoding matrix indicator (PMI) feedback to control the AMAP block. This control information is also sent over the PDCCH to control the inverse UE operation.

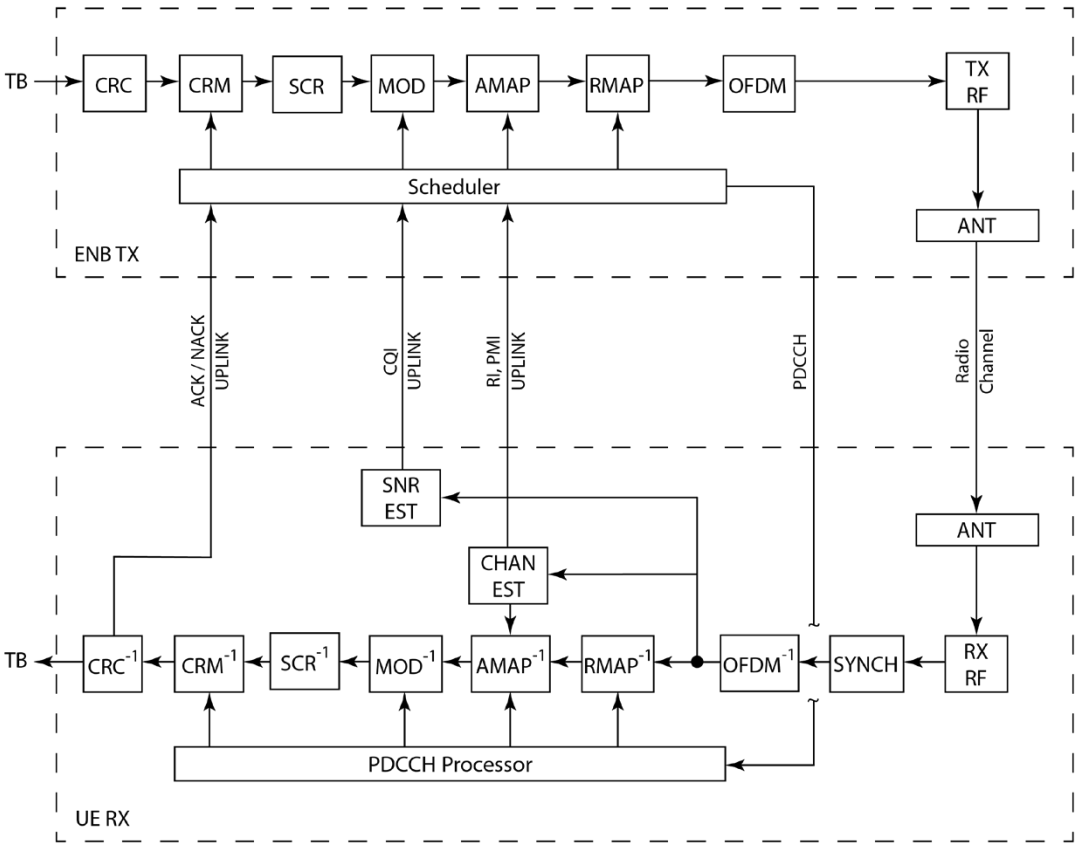

Figure B-2 Signal processing for a single downlink UE PDSCH. Top portion is eNB transmitter signal processing. Bottom portion is UE receiver signal processing.

B.3 Throughput

Maximum throughput can be computed with ETSI 3GPP tables [B-6] summarized in Table B-2. Transport block size (TBS) is the number of bits that can be transmitted in one subframe per 1 ms transmission time interval (TTI). TBS is a function of the number of paired RB and the TBS index which is related to the MCS. Recall that the TB is a MAC entity without the CRC, FEC, or overhead the physical layer adds.

Throughput can also be limited by the UE capability class or "category." Although categories range from 1 to 5, the most common are presently 2, 3, and 4. The main difference between these categories is the amount of "soft" memory available for HARQ retransmission combining (HRC).

Table B-2 ETSI 3GPP tables used to compute maximum data throughput.

Table	Table Identifier	Description
Modulation and TBS index table for PDSCH	Table 7.1.7.1-1	Relates MCS to TBS and TBS index
One-layer TBS table	Table 7.1.7.2.1-1	Relates TBS index and number of paired RBs to TBS for single layer transmission for up to 110 paired RBs and two layer transmission for up to 55 paired RBs.

B.4 References

[B-1] ETSI, "LTE; Evolved Universal Terrestrial Radio Access (E-UTRA); Services provided by the physical layer," ETSI TS 36.302

[B-2] ETSI, "LTE; Evolved Universal Terrestrial Radio Access (E-UTRA); Media Access Control (MAC) protocol specification," ETSI TS 36.321

[B-3] M. Baker, "Signal Structure", Section 6.3 in *LTE, The UMTS Long Term Evolution, From Theory to Practice, Second Edition*, S. Sesia, I. Toufik, and M. Baker editors, John Wiley and Sons, West Sussex, United Kingdom, 2011.

[B-4] D. Hanley,"Codewords and layers and ports, Oh My!", Expert Opinion Blog, LTE University, Sept. 20, 2011, http://lteuniversity.com/get_trained/expert_opinion1/b/donhanley/archive/2011/09/20/codewords-and-layers-and-ports-oh-my.aspx

[B-5] A. Toskala, T. Lunttila, E. Tiirola, K. Hooli, M. Chmiel, and J. Korhonen, "Channel Feedback Report Types in LTE," Section 5.9.6.1 in *LTE for UMTS*, Second Edition, H. Holma and A. Toskala, editors, John Wiley and Sons, West Sussex, United Kingdom, 2011.

[B-6] ETSI TS 36.213, "LTE; Evolved Universal Terrestrial Radio Access (E-UTRA); Physical Layer Procedures," European Telecommunications Standards Institute, Sophia-Antipolis, France.

APPENDIX C: CREATING SNR/CQI/MCS TABLES

The LTE adaptive modulation and coding (AMC) function automatically matches signal modulation order and coding rate to channel quality conditions. In the simulation model, channel quality is evaluated solely on the basis of received SNR. The UE portion of the AMC function measures the received SNR, converts it to CQI, and sends the CQI to the eNB. The eNB portion of the AMC function converts the CQI to the appropriate MCS. The relationship between SNR, CQI, and MCS is dependent on the transmission mode (e.g. diversity or space division multiplexing) and type of propagation channel (e.g. AWGN, frequency flat fading, or frequency selective fading) [C-1].

The AMC table used in this report was populated with SNR, CQI, and MCS values acquired by simulation. Open loop spatial multiplexing transmission mode 3 in an AWGN channel without fading was used to emulate measurement conditions. This Appendix describes the procedure [C-2] used to create the AMC table and presents results for the AWGN channel and 10% first transmission BLER in Table C-2.

C.1 Method

1) Set HARQ retransmissions to 0 so that all metrics are first transmission metrics

2) Fix MCS to the lowest value

3) Measure throughput and BLER over a range of SNR that provides BLER ranging from 0 to 100%.

4) Repeat for all MCS

5) Interpolate SNR at the desired maximum BLER for each MCS. 10% is a typical desired maximum BLER.

6) Create 15 element SNR to CQI table. The rules for assigning CQI are summarized in Table C-1. The first CQI element CQI(0) has an undefined MCS.

7) Create 16 element CQI to MCS table.

Table C-1. Minimum SNR to CQI table rules where n is table index

CQI	**SNR range**	**Note**
0	NA	Out of range
1	$SNR < SNR(1)$	
2-14	$SNR(n-1) \leq SNR < SNR(n)$	**$2 \leq n < 15$**
15	$SNR(15) \leq SNR$	

C.2 Results

Table C-2. CQI, MCS, SNR for AWGN channel and 10% first transmission BLER. Modulation order, TBS index, and TBS taken from [C-3] and [C-4].

Minimum SNR (dB)	CQI	MCS Index	Modulation Order	TBS Index	TBS
-4.7	1	0	2	0	1384
-3.5	2	2	2	2	2216
-2.2	3	4	2	4	3624
-0.9	4	6	2	6	5160
1.0	5	8	2	8	6968
2.8	6	10	4	9	7992
4.1	7	12	4	11	9912
5.9	8	14	4	13	12960
7.3	9	16	4	15	15264
9.5	10	18	6	16	16416
11.2	11	20	6	18	19848
12.6	12	22	6	20	22920
14.8	13	24	6	22	27376
16.8	14	26	6	24	30576
18.0	15	27	6	25	31704

C.3 References

[C-1] C. Mehlfuhrer, M. Wrulich, J. C. Ikuno, D. Bosanka, M. Rupp, "Simulating the Long Term Evolution Physical Layer," in *Proc. of the 17th European Signal Processing Conference*, Glasgow, Scotland, Aug. 24-28, 2009, pp. 1471-1478.

[C-2] M. T. Kawser, N. I. Bin Hamid, M. N. Hasan, M. S. Alam, M. M. Rahman, "Downlink SNR to CQI Mapping for Different Multiple Antenna Techniques in LTE," *International Journal of Information and Electronics Engineering*, Vol. 2, No. 5, Sept. 2012, pp. 757-760.

[C-3] ETSI TS 36.213, Table 7.1.7.1-1 Modulation and TBS Index Table for PDSCH in "LTE; Evolved Universal Terrestrial Radio Access (E-UTRA); Physical Layer Procedures," European Telecommunications Standards Institute, Sophia-Antipolis, France.

[C-4] ETSI TS 36.213, Table 7.1.7.2-1 Transport Block Size Table in "LTE, Evolved Universal Terrestrial Radio Access (E-UTRA); Physical Layer Procedures," European Telecommunications Standards Institute, Sophia-Antipolis, France.

NTIA FORM 29
(4-80)

U.S. DEPARTMENT OF COMMERCE
NATIONAL TELECOMMUNICATIONS AND INFORMATION ADMINISTRATION

BIBLIOGRAPHIC DATA SHEET

1. PUBLICATION NO.	2. Government Accession No.	3. Recipient's Accession No.
TR-19-540		

4. TITLE AND SUBTITLE	5. Publication Date
Interference Protection Criteria Simulation	August 8, 2019
	6. Performing Organization Code NTIA/ITS.T

7. AUTHOR(S)	9. Project/Task/Work Unit No.
Robert J. Achatz and Brent Bedford	
8. PERFORMING ORGANIZATION NAME AND ADDRESS Institute for Telecommunication Sciences National Telecommunications & Information Administration U.S. Department of Commerce 325 Broadway Boulder, CO 80305	3105011-300 6504000-209
	10. Contract/Grant Number.

11. Sponsoring Organization Name and Address	12. Type of Report and Period Covered
National Telecommunications & Information Administration Herbert C. Hoover Building 14th & Constitution Ave., NW Washington, DC 20230	

14. SUPPLEMENTARY NOTES

15. ABSTRACT (A 200-word or less factual summary of most significant information. If document includes a significant bibliography or literature survey, mention it here.)

Interference protection criteria (IPC) determine the interfering signal power a system can tolerate when sharing spectrum with other services. IPC are typically determined by measurements, but good measurements are often hindered by restrictions on equipment availability and inaccessible intermediate signals, performance metrics, and operational parameters. The purpose of this research is to determine if radio system software simulation can accurately emulate these measurements and alleviate their hindrances. Our approach is to use commercial off-the-shelf (COTS) radio system simulator software to model previous IPC measurement test fixtures and compare simulated to measured results. Measurements of mutual interference between SPN-43C radar and LTE systems are compared. The comparison revealed that 1) when the SPN-43C pulse repetition interval was the same as the LTE subframe period SPN-43C interference in the LTE UE was highly dependent on which OFDM word within the LTE subframe the SPN-43C pulse was repeatedly placed on and 2) simulation is more accurate than measurement for IPC tests with fixed threshold radars such as SPN-43C. These revelations show that simulation is a useful addition and potentially viable alternative to IPC measurement.

16. Key Words (Alphabetical order, separated by semicolons)

Citizens Broadband Radio Service, electromagnetic compatibility analysis, interference protection criteria, LTE, radio system software simulation, spectrum engineering, spectrum sharing, surveillance radar

17. AVAILABILITY STATEMENT	18. Security Class. (This report)	20. Number of pages
☒ UNLIMITED.	Unclassified	63
☐ FOR OFFICIAL DISTRIBUTION.	19. Security Class. (This page) Unclassified	21. Price:

NTIA FORMAL PUBLICATION SERIES

NTIA MONOGRAPH (MG)

A scholarly, professionally oriented publication dealing with state-of-the-art research or an authoritative treatment of a broad area. Expected to have long-lasting value.

NTIA SPECIAL PUBLICATION (SP)

Conference proceedings, bibliographies, selected speeches, course and instructional materials, directories, and major studies mandated by Congress.

NTIA REPORT (TR)

Important contributions to existing knowledge of less breadth than a monograph, such as results of completed projects and major activities.

JOINT NTIA/OTHER-AGENCY REPORT (JR)

This report receives both local NTIA and other agency review. Both agencies' logos and report series numbering appear on the cover.

NTIA SOFTWARE & DATA PRODUCTS (SD)

Software such as programs, test data, and sound/video files. This series can be used to transfer technology to U.S. industry.

NTIA HANDBOOK (HB)

Information pertaining to technical procedures, reference and data guides, and formal user's manuals that are expected to be pertinent for a long time.

NTIA TECHNICAL MEMORANDUM (TM)

Technical information typically of less breadth than an NTIA Report. The series includes data, preliminary project results, and information for a specific, limited audience.

For information about NTIA publications, contact the NTIA/ITS Technical Publications Office at 325 Broadway, Boulder, CO, 80305 Tel. (303) 497-3572 or e-mail ITSinfo@ntia.gov.